Petroleum Science 22 (2025) 492–507

Contents lists available at ScienceDirect

Petroleum Science

journal homepage: www.keaipublishing.com/en/journals/petroleum-science

Original Paper

Exceptional functionalized dual-acidic ionic liquid: High-efficiency catalytic reaction medium for oxidation desulfurization

Ran Liu [a, b, c], Chang Wang [b], Qiang Yang [b], Jing-Ran Yang [b], Chen Liu [a, b], Liberty Mguni [a], Xin-Ying Liu [a, b], Ya-Li Yao [a, b, *], Fa-Tang Li [a, b, c, **]

[a] Institute for Catalysis and Energy Solutions, University of South Africa, Johannesburg, 1710, South Africa
[b] International Joint Laboratory of New Energy, College of Chemistry and Pharmaceutical Engineering, Hebei University of Science and Technology, Shijiazhuang, 050018, Hebei, China
[c] Hebei Key Laboratory of Photoelectric Control on Surface and Interface, College of Science, Hebei University of Science and Technology, Shijiazhuang, 050018, Hebei, China

ARTICLE INFO

Article history:
Received 10 March 2024
Received in revised form
8 July 2024
Accepted 8 July 2024
Available online 11 July 2024

Edited by Min Li

Keywords:
Dual-acidic ionic liquid
Catalysis
Oxidation desulfurization
Reactive oxygen species

ABSTRACT

The development of highly active functionalized ionic liquids (ILs) as both extractants and catalysts for use in achieving deep desulfurization continues to pose challenges. In this study, a highly efficient oxidative desulfurization system was constructed, composed of dual-acidic ionic liquids (DILs) and H_2O_2-AcOH. The investigation results of four DILs prepared from different metal chlorides ($[HSO_3C_3NEt_3]Cl$-$MnCl_n$, $MnCl_n$ = $AlCl_3$, $ZnCl_2$, $CuCl_2$, $FeCl_3$) in oxidative desulfurization showed that $[HSO_3C_3NEt_3]Cl-AlCl_3$ had an outstanding catalytic effect and significantly promoted the oxidation of sulfides. With a 0.2 g $[HSO_3C_3NEt_3]Cl-AlCl_3$, the removal rate of dibenzothiophene (DBT) reached 100% in 10 mL model oil under mild conditions at 55 °C for 20 min. The key is its ability to induce the dismutation of superoxide anions ($\bullet O_2^-$), which facilitates the generation of singlet oxygen ($^1O_2$). The efficient oxidation of DBT is accomplished through a predominantly $^1O_2$-mediated non-radical mechanism. $[HSO_3C_3NEt_3]Cl$-$AlCl_3$ serves as a favorable medium for contact to be made between $^1O_2$ and sulfides, which indicates an efficient catalytic-adsorption synergy.

1. Introduction

When sulfur compounds in transportation fuels combust, they generate sulfur oxides, contributing to environmental pollution. Therefore, there is a growing need for stricter regulation of the sulfur levels in fuels (Boshagh et al., 2022a, 2022b; Tanimu et al., 2022). The hydrodesulfurization (HDS) method is commonly used for deep desulfurization of fuels in industry (Liu et al., 2023a, 2023b; Zhou et al., 2024). This method involves breaking the C–S bond to produce H_2S and is effective in eliminating both aliphatic and non-cyclic sulfur compounds, such as sulfides, thiols, disulfides and thiols. However, approximately half of the sulfur-containing compounds in fuel oil belong to the thiophene class, including thiophene (T), benzothiophene (BT), dibenzothiophene (DBT) and their derivatives. Because of their high stability, the bond energies of C–S and C–H in thiophenes are nearly equal, which means the C–S bond is difficult to break and the removal of sulfur via hydrogenation desulfurization is extremely difficult (Salah et al., 2021; Zhu et al., 2021). Therefore, various non-HDS methods have been developed to effectively remove BT, DBT and their derivatives, including extraction desulfurization (EDS) (Aghaei and Sobati, 2022; Wu et al., 2021; Xu et al., 2021b), adsorption desulfurization (ADS) (Ganiyu and Lateef, 2021; Saha et al., 2021; Yin et al., 2022; Luo et al., 2022; Shan et al., 2022; Wang et al., 2022) and oxidation desulfurization (ODS) (Haruna et al., 2022; Shafiq et al., 2021).

The ODS method has been given much attention due to its relatively high efficiency under mild conditions. Hydrogen peroxide (H_2O_2) is known for its environmentally friendly characteristics and is commonly employed as an oxidant in the ODS processes. In desulfurization systems where H_2O_2 serves as the oxidant, the oxidant and the sulfides exist in the non-oil phase and the oil phase, respectively. Therefore, the key challenges to

* Corresponding author.
** Corresponding author.
E-mail addresses: yaoy@unisa.ac.za (Y.-L. Yao), lifatang@126.com (F.-T. Li).

https://doi.org/10.1016/j.petsci.2024.07.012

enhancing the oxidative desulfurization effect are: increasing reactive oxygen species (ROSs) in the reaction system; and ensuring favorable conditions for contact between ROSs and the sulfides distributed in the different phases. This means that catalysts and extractants play a crucial role in removing sulfides. Ionic liquids (ILs) demonstrate many unique advantages in catalytic reactions (Bhutto et al., 2016; Malolan et al., 2021). For instance, their high chemical stability is conducive to the stable progress of catalytic reactions, and their strong structural tunability enables customized catalytic functions to meet diverse catalytic reaction requirements. Additionally, their low volatility and recyclability contribute to reducing environmental pollution and minimizing catalyst loss. Therefore, ILs are widely applied and researched in the field of chemical engineering. One of the hot research areas is the application of ILs in deep desulfurization of fuel oils (Liu et al., 2021). Numerous studies have reported that ILs can function as either the extractant or catalyst, or as both simultaneously, and enable deep desulfurization of fuels (Salah et al., 2021; Aghaei and Sobati, 2022). In 2001, Bösmann et al. (2001) first reported that ILs exhibited a similar polarity to sulfides, and resulted in a significantly higher distribution of coefficients of sulfide compounds in ILs. However, subsequent studies have indicated that achieving deep desulfurization requires an increase in the number of extraction experiments. This leads to an increase in fuel oil losses and an increase in extraction costs (Huang et al., 2004; Li et al., 2010, 2019; Wang et al., 2020a; Nie et al., 2006; Chen et al., 2014; Dharaskar et al., 2013).

In 2003, Lo et al. (2003) first reported a study on oxidative desulfurization using ILs in the presence of oxidants in order to achieve one-step deep oxidative desulfurization. By leveraging the exceptional extraction capacity of ILs for S-compounds, a substantial number of S-compounds could be oxidized in the IL phase. The oxidation of the sulfide compounds resulted in a decrease in the saturation level of sulfides in the ILs (oxidized sulfide products exhibit higher solubility in the ILs). This improved the ability of the ILs to extract sulfides. A number of studies subsequently confirmed that ILs with specific structures serve as the media for oxidation reactions and act as the catalyst in the oxidation of sulfides (Zhao et al., 2007, 2008a; Liu et al., 2018; Li et al., 2009, 2012, 2015a; Wang et al., 2017; Lu et al., 2007; Hao et al., 2019). This accelerates the reaction rate, reduces reaction conditions and achieves one-step deep desulfurization under mild conditions. Therefore, the potential application value of ILs in catalytic oxidative desulfurization is obvious.

The negative aspects of the reaction process include using a high temperature, prolonged reaction time and using a considerable amount of ILs. Additionally, the inherent insolubility between ILs and the oil phase poses challenges. These issues contribute to the high cost of the desulfurization process and prevent it from being adopted in the petroleum industry. For environmental and cost-control purposes, water is the most suitable extractant. However, it is extremely difficult for sulfides to contact oxidants in the aqueous phase, which means achieving satisfactory desulfurization is challenging. A promising research strategy is to use water as the main solvent in the extraction phase to avoid the loss of alkanes in the oil phase while using ILs as the catalysts and extractants to increase the contact of sulfides and oxidants. This approach aims to achieve mild, efficient, cost-effective oxidative desulfurization with minimal use of catalyst and at a low cost. The dual-acidic ionic liquids (DILs) designed in this study provide an ideal pathway to implement this strategy.

This strategy is suggested due to various interaction mechanisms observed between the cations and anions of ILs and aromatic sulfide compounds. These mechanisms encompass several interactions: organic heterocyclic cations and quaternary phosphonium salt cations in ILs with aromatic thioether compounds (such as DBT and dibenzothiophene sulfoxide ($DBTO_2$)) engage in CH–π, π–π, and hydrogen bond interactions. These interactions facilitate the insertion of DBT into the molecular structure of IL (Desai et al., 2022; Raj et al., 2019; Li et al., 2015b; Dharaskar and Sillanpaa, 2018; Dharaskar et al., 2021). Additionally, the quaternary ammonium cations in ILs demonstrate amphiphilic characteristics between the water phase and the oil phase, which prove advantageous for the oxidation of aromatic thioethers (Zhao et al., 2008b, 2009, 2010; Ge et al., 2011). Moreover, the transition metal chlorides (Lewis acids) acting as the anions of ILs can form π-interactions with aromatic sulfides, thereby enhancing the presence of sulfides in the solvent phase (Ban et al., 2013; Wang et al., 2010). Finally, in a reaction system in which H_2O_2 serves as the oxidant, an acidic environment (Brønsted acids and Lewis acids) can facilitate the oxidation reaction, which favors the oxidation of sulfides in the oxidative desulfurization process (Santos et al., 2008; Rodriguez-Gattorno et al., 2009; Dharaskar et al., 2015; Yang et al., 2016; Gui et al., 2010).

After considering these factors, an efficient oxidative desulfurization strategy was devised in this study using a DIL as a catalyst in the H_2O_2-AcOH system. The catalyst design was based on the following factors: Firstly, a suitable level of lipophilicity was achieved by selecting triethylamine butane sulfonate as the ionic liquid cation, which minimizes the loss of ionic liquid in the oil phase. This is because although extending the alkyl chain length of the cation in the IL is beneficial for the desulfurization of aromatic sulfides (Dharaskar et al., 2021; Nie et al., 2013; Li et al., 2015c), excessively long alkyl chains increase the lipophilicity of the ionic liquid, even lead to emulsification of the reaction system, thus leading to an increase in ionic liquid loss (Wang et al., 2020a). Secondly, transition metal chlorides can be used as the anions of the ionic liquid, as they form π complexes with aromatic sulfides and enhance desulfurization efficiency by increasing the Lewis acidity of the ionic liquid (Zhao et al., 2007; Li et al., 2015b; Ban et al., 2013; Wang et al., 2010; Chen et al., 2012). Finally, because of the limited strength of Lewis acids, hydrochloric acid (HCl) was used to acidify the ionic liquid intermediate. This produced a Brønsted acidic ionic liquid intermediate, which interacted with metal chlorides to form Brønsted-Lewis dual-acidic ionic liquids, include triethyl-3-propanesulfonate chloroaluminate ionic liquid ($[HSO_3C_3NEt_3]Cl$-$AlCl_3$), triethyl-3-propanesulfonate chlorozincate ionic liquid ($[HSO_3C_3NEt_3]Cl$-$ZnCl_2$, triethyl-3-propanesulfonate chlorocuprate ionic liquid ($[HSO_3C_3NEt_3]Cl$-$CuCl_2$), and triethyl-3-propanesulfonate chloroferrate ionic liquid ($[HSO_3C_3NEt_3]Cl$-$FeCl_3$).

This study investigated the catalytic performance of the four DILs mentioned above and systematically examined the effects of operating conditions, including reaction temperature, reaction time, catalyst dose, amount of H_2O_2 and AcOH, and stirring rate on the desulfurization rate. Through a series of quenching experiments and electron paramagnetic resonance (EPR) characterization, the reactive oxygen species (ROSs), and their oxidation behavior in the DILs-H_2O_2-AcOH desulfurization system were analyzed. And a possible catalytic desulfurization mechanism was proposed. In addition, the desulfurization effect of DILs on different sulfides and actual diesel was also studied. The good recyclability of DILs highlights their advantages such as stable structure, excellent catalytic performance, and controllable cost. This study was aimed at determining an innovative approach to enhance the efficiency of ILs oxidative desulfurization and advance its feasibility for use in industry.

2. Experiments

2.1. Chemicals and materials

The following materials were procured from Shanghai Aladdin Reagent Co. Ltd: 1,3-propanesultone (AR grade, ≥99%); HCl (37 wt% aqueous solution); triethylamine (AR grade, 99%); acetone (AR grade, ≥97%); anhydrous $ZnCl_2$ (AR grade, 99%); anhydrous $FeCl_3$ (AR grade, 99%); anhydrous $AlCl_3$ (AR grade, 99%); anhydrous $CuCl_2$ (AR grade, 99%); H_2O_2 (AR grade, 30 wt% aqueous solution); *n*-octane (96%, AR grade); thiophene (AR grade, 98%); benzothiophene (AR grade, 98%); 2-methylbenzothiophene (AR grade, 98%); dibenzothiophene (AR grade, 98%); 4,6-Dimethyldibenzothiophene (AR grade); glacial acetic acid (AR grade, 98%); isopropanol (IPA, 99%, AR); 1,4-benzoquinone (p-BQ, 99%, AR); 4-amino-2,2,6,6-tetramethylpiperidine (TEMP, >98%, GC); 5,5-dimethyl-1-pyrroline N-oxide (DMPO, AR grade, 97%).

2.2. Preparation of ILs

The four types of triethylamine-based Brønsted-Lewis acid ionic liquids were prepared as follows: 20.24 g (0.024 mol) of triethylamine, 24.43 g (0.024 mol) of 1,3-propanesultone and 50 mL of acetone were added into a 250 mL three-necked flask and the reaction was carried out at 50 °C for 3 h. The mixture was then vacuum-filtered, washed with acetone three times to remove unreacted impurities, and then vacuum-dried to a constant weight, which yielded a white solid intermediate. Next, 8.86 g of the white solid intermediate and HCl (1:3 M ratio) were combined and added to a 250 mL three-necked flask, and the mixture was reacted at 80 °C for 2 h. Unreacted HCl was then removed by vacuum rotary evaporation, and the product was washed with ethyl acetate three times. This resulted in a pale yellow viscous Brønsted acid ionic liquid $[HO_3SC_3NEt_3]Cl$. Equimolar amounts of $[HO_3SC_3NEt_3]Cl$ and metal chlorides ($AlCl_3$, $ZnCl_2$, $CuCl_2$, $FeCl_3$) were then added to a 250 mL three-necked flask. The mixture was reacted at 70 °C for 1.5 h. The resulting product was subjected to vacuum rotary evaporation to remove most of the water and then dried under vacuum to constant weight. This yielded the Brønsted-Lewis acid ionic liquids $[HSO_3C_3NEt_3]Cl$-$ZnCl_2$, $[HSO_3C_3NEt_3]Cl$-$AlCl_3$, $[HSO_3C_3NEt_3]Cl$-$CuCl_2$ and $[HSO_3C_3NEt_3]Cl$-$FeCl_3$. The synthetic pathway for triethylamine-based Brønsted-Lewis acid ionic liquids is illustrated in Scheme S1.

2.3. Characterization and analysis

Fourier Transform Infrared Spectrometer (FT-IR) was used to determine the surface functional groups of the Brønsted-Lewis acid ionic liquids $[HSO_3C_3NEt_3]Cl$-$AlCl_3$, $[HSO_3C_3NEt_3]Cl$-$ZnCl_2$, $[HSO_3C_3NEt_3]Cl$-$CuCl_2$ and $[HSO_3C_3NEt_3]Cl$-$FeCl_3$ using a Bruker Vertex70 spectrometer (FTS-135 Fourier Transform Infrared Spectrometer, BIO-RAD, USA) over the 400–4000 cm^{-1} wavenumber range. The Brønsted acidity was measured using a pH meter (EL20 laboratory pH meter, Mettler-Toledo Instruments (Shanghai) Co. Ltd). Using pyridine as a probe, the strength of Lewis acidity of the four DILs was compared and characterized by infrared absorption spectroscopy (FTS-135 Fourier Transform Infrared Spectrometer, BIO-RAD, USA). The characterization of the structural composition of the ionic liquid intermediate $[HSO_3C_3NEt_3]Cl$ was determined by ^1H nuclear magnetic resonance (NMR) using a Bruker AVANCE 500 MHz Spectrometer (Bruker, Switzerland). The ROSs generated during the sulfide oxidation reaction were detected using a German Bruker A300 Electron Paramagnetic Resonance (EPR) spectrometer.

2.4. Desulfurization experiments

The five different types of model oil with 1000 ppm S-content were prepared by dissolving 0.934 g thiophene (T), 1.477 g benzothiophene (BT), 1.666 g 2-methyl benzothiophene (2-MBT), 2.073 g dibenzothiophene (DBT) and 2.391 g 4,6-dimethyl dibenzothiophene (4,6-DMDBT) in 500 mL *n*-octane. The original actual diesel had a S-content of 726 ppm. For the desulfurization experiment, 10 mL model oil or actual diesel was mixed with a predetermined amount of ILs, H_2O_2 and AcOH, and added to a three-necked flask under vigorous stirring. It was reacted for a predetermined time and an oil bath was used to adjust the reaction temperature. During the reaction, the sulfur content in the upper phase was periodically separated and analyzed using a sulfur analyzer. The sulfur content was measured using a THA-2000S Ultraviolet Fluorescence Sulfur Analyzer (Taizhou Jin Hang Analytical Instrument Co. Ltd, China). The sulfur types were determined using a GC-FPD (SP-3420A, Beijing Beifen Ruili Analytical Instrument Co. Ltd, China).

3. Results and discussion

3.1. Characterization of ionic liquids

The four types of DILs-$[HSO_3C_3NEt_3]Cl$-$AlCl_3$, $[HSO_3C_3NEt_3]Cl$-$ZnCl_2$, $[HSO_3C_3NEt_3]Cl$-$FeCl_3$ and $[HSO_3C_3NEt_3]Cl$-$CuCl_2$ were analyzed by means of FT-IR spectroscopy. The results are shown in Fig. 1(a), and the following can be seen: the anti-symmetric stretching vibration peak appears at about 2988 cm^{-1}, which belongs to C–H on CH_3 and CH_2. The bending vibration peak of C–H on CH_3 appears at about 1488 cm^{-1}. The stretching vibration peak of S=O appears at about 1148 cm^{-1}. The S–O stretching vibration peak appears at about 729 cm^{-1}. The stretching vibration peak of S–O and the stretching vibration peak of N–C appear at about 1033 cm^{-1}. The characteristic absorption peak that matches the target product appears in the infrared spectrum. The intermediate $[HSO_3C_3NEt_3]Cl$ was characterized by ^1H NMR. $[HO_3SC_3NEt_3]Cl$: ^1H NMR (500 MHz, D_2O) d: 1.265–1.293 (m, 9H, $-CH_2-CH_3$), d: 2.114–2.148 (d, 2H, $-CH_2-CH_2-$), d: 2.966–2.994 (d, 2H, $-H-SO_3$), d: 3.291–3.365 (m, 8H, $-N-CH_2-$) and d: (s, 1H). The synthesized substance served as the intermediate $[HSO_3C_3NEt_3]Cl$. The acidity of the catalyst could potentially influence the oxidation of sulfur-containing compounds. Aqueous solutions of four DILs with mass fractions of 1%, 2%, 3%, 4%, and 5% were prepared, respectively, and their Brønsted acidity was measured using a pH meter. The results are presented in Table 1. It shows that the Brønsted acidity of the four ionic liquids at equivalent mass concentrations is closely comparable. However, a discernible order of acidity strength is seen: $[HSO_3C_3NEt_3]Cl$-$AlCl_3$ > $[HSO_3C_3NEt_3]Cl$-$ZnCl_2$ > $[HSO_3C_3NEt_3]Cl$-$FeCl_3$ > $[HSO_3C_3NEt_3]Cl$-$CuCl_2$. This trend correlates with the subsequent desulfurization experiments involving the four DILs and reflects their catalytic oxidative performance.

The Lewis acidity of the synthesized ionic liquids is shown in Fig. 1(b). The presence of Lewis acidity in the ionic liquids is indicated by the absorption peak around 1450 cm^{-1}. The characteristic absorption peak of pyridine appears at 1437.95 cm^{-1}. Upon coordination complex formation between pyridine and Lewis acid, the characteristic peak shifts to a higher wave number, i.e. about 1450 cm^{-1}. The extent of the shift in the characteristic peak of the pyridine complex indicates that the Lewis acidity order of the four ILs is as follows: $[HSO_3C_3NEt_3]Cl$-$FeCl_3$ > $[HSO_3C_3NEt_3]Cl$-$AlCl_3$ > $[HSO_3C_3NEt_3]Cl$-$ZnCl_2$ > $[HSO_3C_3NEt_3]Cl$-$CuCl_2$.

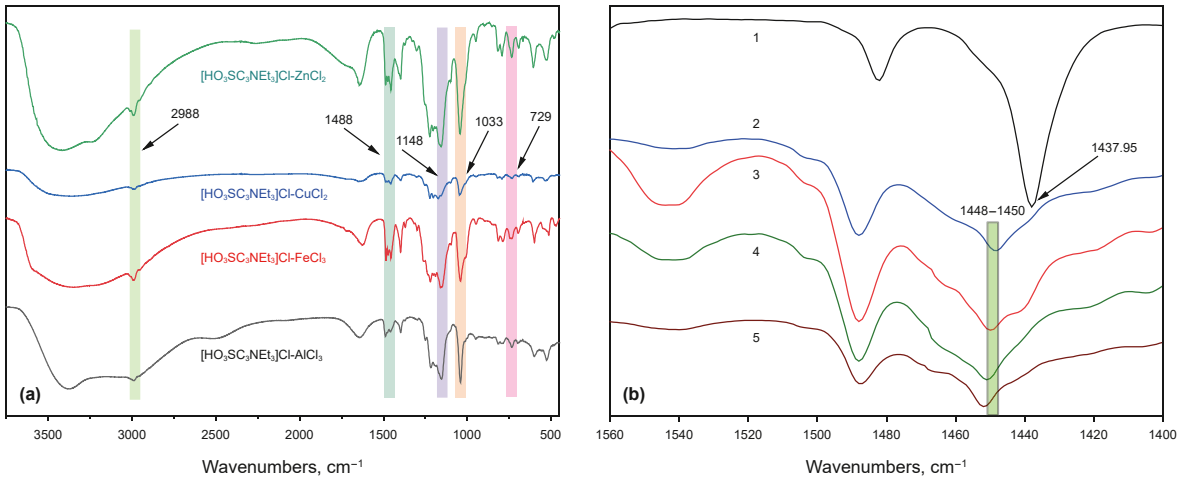

Fig. 1. **(a)** FT-IR spectra of four Brønsted-Lewis acid ionic liquids. **(b)** FT-IR spectra of the Lewis acidity using the pyridine probe method. 1-Pyridine. 2-[$HSO_3C_3NEt_3$]Cl-$CuCl_2$.3-[$HSO_3C_3NEt_3$]Cl-$ZnCl_2$. 4-[$HSO_3C_3NEt_3$]Cl-$AlCl_3$. 5-[$HSO_3C_3NEt_3$]Cl-$FeCl_3$.

Table 1
Acidity of the aqueous solutions of four Brønsted-Lewis acid ionic liquids with different mass fractions (wt.%).

Ionic liquid	pH				
	1 wt%	2 wt%	3 wt%	4 wt%	5 wt%
[$HSO_3C_3NEt_3$]Cl-$AlCl_3$	2.56	2.31	2.11	1.91	1.74
[$HSO_3C_3NEt_3$]Cl-$ZnCl_2$	2.54	2.26	2.07	1.83	1.68
[$HSO_3C_3NEt_3$]Cl-$FeCl_3$	2.30	2.01	1.81	1.68	1.46
[$HSO_3C_3NEt_3$]Cl-$CuCl_2$	2.27	1.95	1.76	1.60	1.37

3.2. Effect of DBT removal using various desulfurization systems

The desulfurization results obtained when using various reaction systems are shown in Fig. 2. Reaction system I comprised H_2O_2, AcOH and model oil. The DBT removal rate was only 23.8%, at a temperature of 55 °C and a reaction time of 20 min. This indicates that, in the absence of a catalyst, the H_2O_2-AcOH system struggled to achieve satisfactory desulfurization results. Reaction system II involved removing DBT through extraction from 10 mL of model oil using four ILs. The DBT removal efficiency ranged from 4% to 6%. This indicates that the extraction efficiency of ILs for DBT is limited. Reaction system III comprised ILs and AcOH. The rate of removal of DBT obtained from the four kinds of ILs ranged from 5% to 8%. The results indicate that adding AcOH just slightly increase the efficiency of ILs extracting DBT in the absence of H_2O_2. In reaction system IV (IL and H_2O_2), when using the same reaction conditions, efficiency in removing DBT increased from 8% to 14% for the four types of ILs. The experimental results indicate that with the weak interaction between the ILs and DBT, a very small amount of DBT was oxidized by H_2O_2, and led to a slight increase in the desulfurization rate. However, due to the inherent challenges of direct oxidation of DBT by H_2O_2, the improvement in the desulfurization rate was constrained. When ILs, H_2O_2 and AcOH were employed concurrently in reaction system V, noticeable disparities were revealed in efficiency in removing DBT by the four types of ILs. When ILs [$HSO_3C_3NEt_3$]Cl-$AlCl_3$ and [$HSO_3C_3NEt_3$]Cl-$ZnCl_2$ acted as the catalysts, the DBT removal rate increased significantly to 100% and 91.2%, respectively, within 20 min. In contrast, when [$HSO_3C_3NEt_3$]Cl-$CuCl_2$ and [$HSO_3C_3NEt_3$]Cl-$FeCl_3$ were used as the catalyst, no improvement was seen with DBT removal efficiency. In fact, the rates recorded for [$HSO_3C_3NEt_3$]Cl-$CuCl_2$ and [$HSO_3C_3NEt_3$]Cl-$FeCl_3$ were lower than in the presence of only H_2O_2 and AcOH, i.e. 14.6% and 13.5%, respectively. The reasons for this result may be explained as follows.

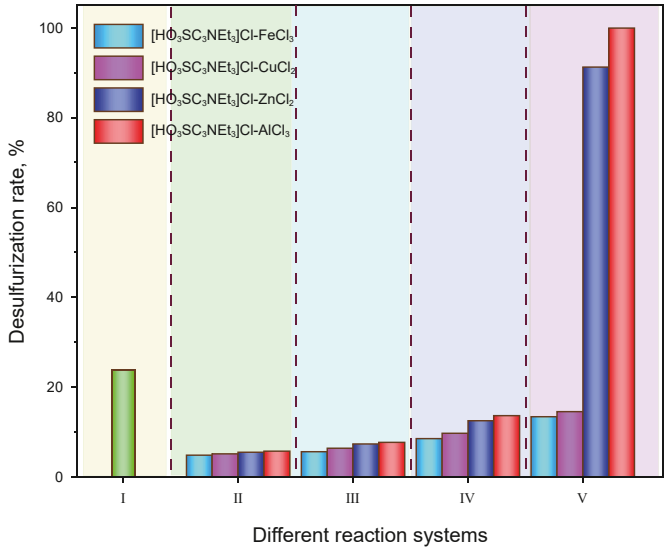

Fig. 2. Removal of DBT using various desulfurization systems. Conditions: T = 55 °C; m(ILs) = 0.2 g; V (model oil) = 10 mL; V (H_2O_2) = 1.0 mL; V (AcOH) = 2.0 mL; t = 20 min; stirring rate = 200 r/min; DBT (1000 ppm) in n-octane. I: H_2O_2+AcOH + model oil; II: ILs (1 mL) + model oil; III: ILs + AcOH + model oil; IV: ILs + H_2O_2+model oil; V: ILs + H_2O_2+AcOH + model oil.

In the [$HSO_3C_3NEt_3$]Cl-$FeCl_3$-H_2O_2-AcOH system, H_2O_2 and AcOH generated peracetic acid (PAA), which then decomposed to hydroperoxyl radicals (HO_2•) and CH_3CO•. Fe^{3+} can react with HO_2• to produce oxygen (O_2) (Bhasarkar et al., 2013). This inevitably leads to the PAA being consumed, which inhibits subsequent oxidation of DBT and results in reduced desulfurization efficiency. The mechanism is expressed in Eqs. (1)–(4). When Fe^{3+} is introduced as the starting reactant, in the absence of AcOH, Fe^{3+} reacts with H_2O_2 as per (Eqs. (1)–(3)):

$$Fe^{3+} + H_2O_2 \rightarrow Fe^{2+} + HO_2\bullet + H^+ \quad (1)$$

$$Fe^{2+} + H_2O_2 \rightarrow Fe^{3+} + HO\bullet + OH^- \quad (2)$$

Equations (1) and (2) reactions are combined as follows:

$$Fe^{3+} + 2H_2O_2 \rightarrow Fe^{3+} + HO_2\bullet + HO\bullet + H_2O \quad (3)$$

When AcOH was added, it had three effects. Firstly, AcOH reacts with H_2O_2 to generate a significant amount of PAA. The release of a substantial amount of $HO_2\bullet$ from PAA can inhibit the progress of Eq. (1). Secondly, AcOH can be oxidized by highly reactive HO• into low-molecular inorganic substances such as CO_2 and H_2O. Thirdly, $HO_2\bullet$ released from PAA can react rapidly with Fe^{3+}, which renders the $HO_2\bullet$ ineffective and leads to the release of O_2. The reaction is expressed in Eq. (4).

$$Fe^{3+} + HO_2\bullet \rightarrow Fe^{2+} + O_2\uparrow + H^+ \quad (4)$$

The extensive consumption of PAA led to a very low oxidative desulfurization efficiency of DBT when $[HSO_3C_3NEt_3]Cl$-$FeCl_3$ was used as the catalyst (Fig. 2V), as suggested by the experimental results (Eq. (4)). Vigorous bubble formation was observed within a short reaction time after adding the ionic liquid $[HSO_3C_3NEt_3]Cl$-$FeCl_3$ (as the catalyst) to the reaction system. This was due to the decomposition of PAA which leads to the production of O_2 catalyzed by Fe^{3+}. The lower desulfurization efficiency of IL $[HSO_3C_3NEt_3]Cl$-$CuCl_2$ may be due to the same reason as shown with $[HSO_3C_3NEt_3]Cl$-$FeCl_3$. In addition, due to the catalytic effect of Cu^{2+}, there was a noticeable color change in the oxidation system before and after the reaction, when $[HSO_3C_3NEt_3]Cl$-$CuCl_2$ was used as the catalyst (See Fig. S1). Cu^{2+} can catalyze the decomposition of H_2O_2, as per Eq. (5), which is detrimental to the oxidation reaction.

$$H_2O_2 \xrightarrow{Cu^{2+}} H_2O + O_2\uparrow \quad (5)$$

Consequently, further investigation into the catalytic performance of ILs $[HSO_3C_3NEt_3]Cl$-$AlCl_3$ and $[HSO_3C_3NEt_3]Cl$-$ZnCl_2$ in the H_2O_2-AcOH oxidative desulfurization system was then done and discussed below.

3.3. Analysis of ROSs and the mechanism involved in DBT oxidation

The experiment results shown in Fig. 2 indicated that after adding $[HSO_3C_3NEt_3]Cl$-$AlCl_3$ or $[HSO_3C_3NEt_3]Cl$-$ZnCl_2$ to the H_2O_2-AcOH oxidation system, the oxidation efficiency of DBT increased significantly compared to the method involving only H_2O_2 and AcOH. This confirms that the addition of either $[HSO_3C_3NEt_3]Cl$-$AlCl_3$ or $[HSO_3C_3NEt_3]Cl$-$ZnCl_2$ in the H_2O_2-AcOH atmosphere enhance the oxidative activity of the reaction system, which may due to the generation of some ROSs.

In the H_2O_2 activation system, there may be ROSs, such as H_2O_2, organic peroxides (ROOH), superoxide anion radicals ($\bullet O_2^-$), hydroxyl radicals (•OH) or singlet oxygen ($^1O_2$). These are often used as the oxidant in many reactions, and exhibit high oxidation efficiency (Ling et al., 2022; Zhu et al., 2020; Hodges et al., 2018; Xing et al., 2021; Xu et al., 2021a; Eugene and Guzman, 2019; Ji et al., 2023). ROSs can be determined by means of capture/quenching experiments and EPR (Wang et al., 2011; Ji et al., 2021). Therefore, it was important to identify ROSs during the oxidation reaction in this study and to analyze the source of various ROSs and their role in the process. This analysis was aimed at providing the key information required to determine the mechanism involved in the oxidation of DBT.

3.3.1. Identification of ROSs in the reaction system by means of capture/quenching experiments and EPR detection

Different kinds of capture or quenching agents can be used to selectively scavenge the oxidative ability of one or some of the ROS species, hereby, the oxidizing capacity of the system will be decreased accordingly (Wang et al., 2011; Ji et al., 2021). Therefore, by analyzing the changes of the oxidative desulfurization capacities during desulfurization runs with adding different capture agents in the oxidative system, the category of the ROSs can be identified.

Table 2 compares the DBT removal rates when using different capture or quenching agents in the DIL-H_2O_2-AcOH oxidation. When using IPA as the capture agent for •OH, the decrease in DBT removal rate was not significant. The DBT removal rate remained above 90% in the DIL-H_2O_2-AcOH oxidation system. The results indicated that capturing •OH has a limited inhibitory effect on the oxidation of DBT, so •OH is not the main ROSs for DBT oxidation. On the other hand, when using p-BQ as the capture agent for $\bullet O_2^-$, the DBT removal rate still remained above 80% in the DIL-H_2O_2-AcOH oxidation system. The reason for the lack of significant decrease in DBT removal rate is not due to the absence of $\bullet O_2^-$ in the system (as confirmed by Fig. 3(b)), but rather due to the low solubility of p-BQ in water. This difficulty leads to significant challenges for p-BQ to capture $\bullet O_2^-$ in the aqueous phase of the reaction system, resulting in the conversion of $\bullet O_2^-$ to $^1O_2$, which further oxidizes DBT. However, when DMPO was used to capture •OH and $\bullet O_2^-$ simultaneously, the desulfurization rate decreased to below 20%, which is significantly lower than when using p-BQ and IPA as quencher. Furthermore, when L-Histidine and TEMP were employed as the quencher and capture agent for $^1O_2$, respectively, the desulfurization rate decreased even more, dropping to below 15%. This suggests that $^1O_2$ is the primary ROSs responsible for the oxidation of DBT. The decrease in the DBT removal rate when DMPO was used as a scavenger is attributed to the capturing of •OH and $\bullet O_2^-$. The quenching of •OH and $\bullet O_2^-$ leads to the obstruction of the oxidation of DBT. Since $\bullet O_2^-$ is the precursors of $^1O_2$, the addition of DMPO inhibits the production of $^1O_2$, hereby, drops the desulfurization rates. It can therefore be concluded that the oxidative system contains active oxygen species, such as •OH, $\bullet O_2^-$ and $^1O_2$, with $^1O_2$ being the predominant active oxygen species.

Our experimental results show that although the presence of DMPO and TEMP both significantly reduces the DBT removal rate, the DBT removal rate in the presence of DMPO (approximately 16%) is relatively higher than that in the presence of TEMP (approximately 2%). This indicates that $\bullet O_2^-$ in the reaction system is not completely captured by DMPO, leading to a small amount of DBT oxidation. It is important to note that DMPO can bind with water in the presence of water, thereby reducing the efficiency of DMPO in capturing $\bullet O_2^-$. Since our research experiments were conducted in an aqueous solution system, the inevitable competition between DMPO and water leads to the possibility of a small amount of $\bullet O_2^-$ being converted to $^1O_2$, thus slightly increasing the DBT removal rate compared to the case of TEMP presence. More details refer to the pathways to produce $^1O_2$ are addressed in Section 3.3.2.

In order to substantiate this conclusion, EPR technology was used to further investigate the existence of three ROSs when using DMPO and TEMP as spin-trapping reagents for the capture of •OH or $\bullet O_2^-$ and $^1O_2$, respectively (Khan, 1977; Liu et al., 2023c). Since using $[HSO_3C_3NEt_3]Cl$-$AlCl_3$ and $[HSO_3C_3NEt_3]Cl$-$ZnCl_2$ have the same effect on desulfurization in this oxidation system, EPR detection was performed in the presence of only $[HSO_3C_3NEt_3]Cl$-$AlCl_3$. Fig. 3(a), (b) and 3(c) provide the signals of TEMP-$^1O_2$, DMPO-$\bullet O_2^-$ and DMPO-•OH, respectively, and confirm the presence of these three active oxygen species in the reaction system.

A comparison of the intensity level of the signals revealed that the $^1O_2$ signal peak is the strongest, followed by •OH, then $\bullet O_2^-$. This

Table 2
The effect that different quenchers and capture agents have on the removal of DBT and the ROSs detection results.

Quencher/Capture agent		ROSs	DBT removal rate in different reaction system		ROS apparent oxidative action
			$[HSO_3C_3NEt_3]Cl$-$AlCl_3$-H_2O_2-A_COH	$[HSO_3C_3NEt_3]Cl$-$ZnCl_2$-H_2O_2-A_COH	
IPA	Quencher	•OH	94.9%	91.1%	ineffective
p-BQ		$•O_2^-$	84.8%	83.2%	ineffective
L-Histidine		$^1O_2$	12.3%	10.1%	effective
DMPO	Capture agent	•OH and $•O_2^-$	16.3%	17.8%	effective
TEMP		$^1O_2$	2.1%	5.5%	effective

Conditions: $T = 55$ °C; m(IL) = 0.2 g; V (model oil) = 10 mL; V (H_2O_2) = 1.0 mL; V (AcOH) = 2.0 mL; n (quencher/capture agent) = 9.79×10^{-3} mol; t = 20 min; stirring rate = 200 r/min; DBT (1000 ppm) in n-octane.

suggests that the concentration of these three active oxygen species in the reaction system follows the order of $^1O_2$ > •OH > $•O_2^-$. Therefore, it can be preliminarily inferred that a high concentration of $^1O_2$ species serves as the primary oxidative species for DBT oxidation in the system, and completes the non-radical oxidation of DBT. •OH and $•O_2^-$ are present in the system, but are not the main active oxygen species responsible for DBT oxidation.

Based on the EPR detection results, the production of active oxygen species, such as $^1O_2$, •OH and $•O_2^-$, and their concentrations in relation to oxidation behavior was further analyzed. This analysis was done to better understand the formation mechanism of the ROSs and the oxidation process of DBT in the system.

3.3.2. ROSs generation mechanism and the oxidation process of DBT in the DIL-H_2O_2-AcOH reaction system

Based on the above results, a thorough analysis of the mechanisms underlying the generation of the three ROSs in the H_2O_2-AcOH system ($^1O_2$, •OH and $•O_2^-$) was considered necessary, as well as an analysis of their relationship between concentration and oxidation behavior. In the DIL, the coexistence of Brønsted acids and Lewis acids facilitates the production of PAA and $HO_2•$ in the reaction system. These peracids serve as precursors to various ROSs, and their generation occurs through a series of pathways (Rodriguez-Gattorno et al., 2009; Gui et al., 2010). According to Hao et al. (2019) and Bhasarkar et al. (2013), potential pathways include:

$$CH_3COOH + H_2O_2 \rightarrow CH_3COOOH + H_2O \quad (6)$$

$$CH_3COOOH \rightarrow CH_3CO• + HO_2• \quad (7)$$

$$HO_2• \rightarrow •O_2^- + H^+ \quad (8)$$

Equation (8) shows that the conversion reaction between $•O_2^-$ and $HO_2•$ is a reversible reaction. In fact, $•O_2^-$ is easily protonated in an acidic solution to yield $HO_2•$ (Wang et al., 2011), so this serves as evidence that there is more $HO_2•$ than $•O_2^-$ present in this oxidation system. Furthermore, due to the low solubility of p-BQ in water, it is challenging for p-BQ to capture the $•O_2^-$ present in the aqueous phase of the reaction system. This could explain why p-BQ did not reduce the desulfurization rate significantly when used as an $•O_2^-$ scavenger, i.e. it only decreased from 100% to below 85% (Table 2). Fig. 3(b) shows that the signal intensity of $•O_2^-$ is the weakest.

The generation of •OH in the system is attributed to the reaction between $HO_2•$ and H_2O_2 (Bhasarkar et al., 2013), as shown in Eq. (9).

$$HO_2• + H_2O_2 \rightarrow •OH + H_2O + O_2 \quad (9)$$

Although •OH can be generated in the system, •OH will react with $CH_3CO•$ to form AcOH (Bhasarkar et al., 2013), as shown in Eq. (10). However, •OH can oxidize AcOH directly into low-molecular-weight inorganic substances, such as CO_2 and H_2O. This inevitably results in non-main reaction consumption of •OH in the reaction system, leading to IPA as an •OH scavenger not significantly reducing the desulfurization rate, only reducing it from 100% to below 95%. Additionally, •OH has a very short lifetime in water (nanoseconds), making it difficult to give a significant oxidative effect on DBT. Moreover, the detection results shown in Fig. 3 indicate that the concentration of •OH is higher than that of $•O_2^-$, but slightly lower than that of $^1O_2$.

$$•OH + CH_3CO• \rightarrow CH_3COOH \quad (10)$$

Another matter to consider is that the generation of $^1O_2$ in this oxidation system may be because of a complex radical conversion process occurring during the reaction processes. It is hard to provide the exact pathways for the generation of $^1O_2$, but we can speculate on two possible mechanisms: one is the $^1O_2$ produced by the oxidation of $•O_2^-$ (Ji et al., 2021); the other is that the $•O_2^-$ decays via the second-order reaction and produces H_2O_2 and $^1O_2$ (Khan, 1977; Zhang et al., 1999; Konovalova et al., 2004). In this research, it is more likely that the $•O_2^-$ decayed to produce $^1O_2$, as per Eq. (11).

$$HO_2• \Big/ •O_2^- + HO_2• \Big/ •O_2^- \rightarrow H_2O_2 + 3^1O_2 \quad (11)$$

Equation (11) is favored due to the presence of a large amount of $HO_2•$, which makes it easier to proceed to the right-hand side of equation. A comparison of the intensity of the signal peaks in Fig. 3(c) suggests that Eq. (11) occurs more easily than Eqs. (8) and (9). Therefore, it can be concluded that Eqs. (8), (9) and (11) all occur simultaneously in the oxidation system, with Eq. (11) being the dominant one. When DMPO was used as the scavenger, the quenching of •OH and $•O_2^-$ inhibited the generation of $^1O_2$, which resulted in a significant reduction in the desulfurization rate. The experimental results when using DMPO as the scavenger confirm a significant reduction in the desulfurization rate to below 20%, which verifies this mechanism (Table 2). Furthermore, when L-Histidine and TEMP were employed as the quencher and capture agents for $^1O_2$, respectively, the desulfurization rate of DBT decreased even more, dropping to below 10%. This indicates that $^1O_2$ functions as the primary ROS responsible for oxidizing DBT. In summary, these analysis results suggest that $^1O_2$ is the main ROS responsible for oxidizing DBT.

It is worth noting that the role of DIL was not reflected in the above-mentioned ROSs generation pathway, so in theory, the above series of reactions can proceed even without DIL catalysts. However, as evidenced by the results seen for the different reaction systems in Fig. 2, relying solely on the above pathway to generate $^1O_2$ is therefore insufficient to achieve effective oxidative desulfurization under such mild conditions. Therefore, it can be proven that the addition of DIL does change or facilitate the above reaction process. The research results shown in Fig. 2 also suggest that in the absence of AcOH, the catalytic effect of DIL ($[HSO_3C_3NEt_3]Cl$-$AlCl_3$) on H_2O_2 ODS is low, i.e. only 14%. This indicates that DIL

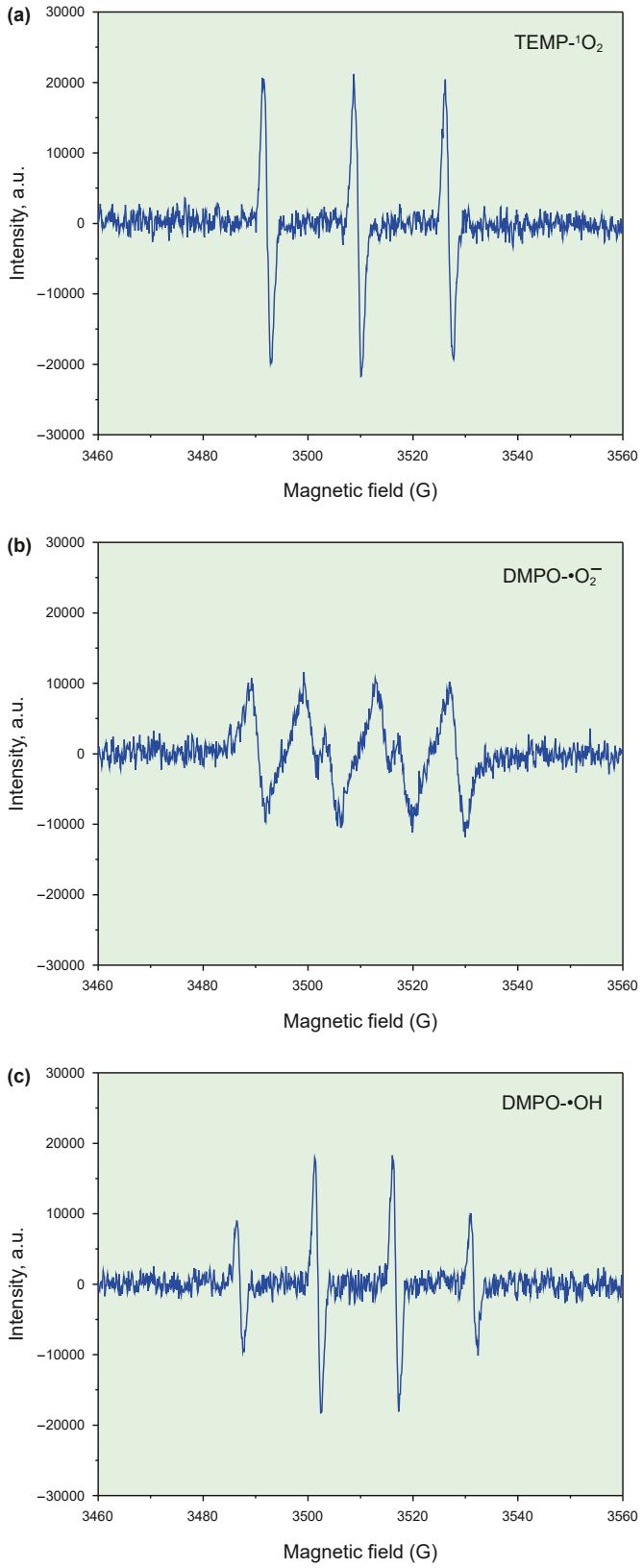

Fig. 3. EPR signals for **(a)** TEMP-$^1O_2$ adducts; **(b)** DMPO-•O_2^- adducts, and **(c)** DMPO-•OH adducts over $[HSO_3C_3NEt_3]Cl$-$AlCl_3$-H_2O_2-AcOH system.

($[HSO_3C_3NEt_3]Cl$-$AlCl_3$) cannot activate H_2O_2 directly to produce ROSs. However, adding AcOH results in desulfurization efficiency increasing significantly, as it reaches almost 100%. This suggests that DIL ($[HSO_3C_3NEt_3]Cl$-$AlCl_3$) plays a role in activating various ROSs that are formed in the H_2O_2-AcOH system, which creates an alternative pathway for $^1O_2$ generation.

Mourad et al. (2019) reported that ILs that contain weak Lewis acidic cations lower the reaction barrier of $^1O_2$ significantly and induce the dismutation of superoxide to form $^1O_2$ when combined with strong Lewis acids. Therefore, we hypothesized that, when induced by DIL, the dismutation reaction of •O_2^- is the main driving force behind $^1O_2$ being generated in the system. According to the report by Mourad et al. (2019): weak Lewis acid alone does not induce dismutation; but when combined with strong Lewis acid, it causes the dismutation of superoxide and the formation of $^1O_2$. Thus, to prevent the generation of $^1O_2$, ILs containing Lewis acids should not be used as additives. However, for this study, DIL which can promote $^1O_2$ generation indirectly was advantageous for the oxidation reaction of DBT. Therefore, the DIL that were designed feature both weak Lewis acidic cation and strong Lewis acidic anion, which allowed for reasonable inference to be made that the DIL induces the dismutation of •O_2^-, which promotes the generation of $^1O_2$. However, the intrinsic mechanism of how the Lewis acids in the DIL lead to the dismutation of superoxide still requires in-depth research.

In addition, as the $^1O_2$ and DBT that serve as the reaction substrates are distributed in immiscible two phases, an appropriate reaction medium is needed to facilitate their reaction. The DIL prepared in this study can provide a suitable reaction medium, as the triethylamine-based cation in the DILs exhibits lipophilicity, which enables it to enter the organic phase and interact with DBT. Unlike traditional phase-transfer catalysts with tetrabutyl structures, the ethyl group in this cation is less hydrophobic than butyl, but it generates minimal steric hindrance, which makes it more conducive to interaction with DBT.

Simultaneously, the hydrophilic nature of the butylsulfonic acid moiety in the cation (like an anchor) retains it in the aqueous phase, while triethylamine can enter the oil phase, which ensures stable IL at the interface between the aqueous phase and the oil phase. This stable presence acts as a bridge that undoubtedly enhances the contact between DBT and the oxidizing agents in the aqueous phase, thereby promoting the biphasic reaction between DBT and ROSs. Additionally, the metal chloride component as the anion of the DIL exhibits a strong ability to accept electrons, which increases the positive charge on the cation of the DIL (i.e. it enhances the positive charge on nitrogen). On the other hand, DBT carries lone pair electrons on sulfur, which results in stronger interaction between the cation of the DIL and DBT (Li et al., 2015b).

Transition metals can form π−π complex with aromatic sulfur compounds in adsorption desulfurization; however, this mechanism-based adsorption desulfurization process generally exhibits low desulfurization efficiency. It is suitable for the adsorption between solid substances and aromatic sulfur compounds, but it performs poorly in terms of adsorption between liquid-liquid phases. Therefore, it can be inferred that the interaction between the DIL and DBT is primarily due to the interaction between the cationic component and DBT. Furthermore, under identical reaction conditions, the superior desulfurization performance of $[HSO_3C_3NEt_3]Cl$-$AlCl_3$ compared to $[HSO_3C_3NEt_3]Cl$-$ZnCl_2$ can be attributed to the higher Brønsted and Lewis acidity of $[HSO_3C_3NEt_3]Cl$-$AlCl_3$. Hence, it is more conducive to promoting the generation of ROSs in the reaction system.

Based on the above analysis, the oxidation of DBT undergoes a free radical-guided non-radical reaction process, and this study determined that the mechanism underlying the oxidation process

of DBT is as follows. The designed DIL effectively promotes the generation of peroxides in the reaction system, thereby facilitating the production of more ROSs acting as active agents for DBT oxidation. The binding of the weak Lewis acidic cations and strong Lewis acidic anions in DIL induces the dismutation of $\bullet O_2^-$, which promotes the generation of $^1O_2$ and establishes a novel pathway for singlet oxygen production. The generated $^1O_2$ was identified as the primary ROS responsible for DBT non-radical oxidation in this pathway.

The triethylamine moiety of the cation in the DIL exhibits good lipophilicity, while the butyl sulfonic acid segment exhibits excellent hydrophilicity, which acts as an anchor that allows the DIL to exist stably at the interface between the oil and water phases. Additionally, the metal chloride component in the anion of the DIL shows a strong electron-accepting ability that increases the positive charge on the cation. This further enhances the interaction between the ionic liquid and DBT to effectively promote more thorough contact between DBT and the oxidizing species in the aqueous phase. Because of these synergistic effects, mild and efficient oxidation of DBT was achieved in this study. The probable pathway for the oxidation reaction of DBT in the DIL-H_2O_2-AcOH reaction system is illustrated in Fig. 4.

3.4. Effect of reaction conditions on DBT removal

According to the research results detailed in the previous section, $[HSO_3C_3NEt_3]Cl\text{-}AlCl_3$ delivers the highest sulfur removal performance. Therefore, it was chosen for a series of parallel experiments that were done to investigate the effect of different reaction conditions on desulfurization performance.

The effect that different doses of DIL have on the removal of DBT is shown in Fig. 5(a). DBT removal was only 64.9% after 20 min with a catalyst dose of 0.1 g. However, extending the reaction time to 30 min increased the desulfurization rate to 84.5%. With a dose of DIL 0.2 and 0.3 g and a reaction time of 10 min, the DBT removal rate can reach to 42.4% and 52.3%, respectively. With a reaction time of 20 min, a removal rate of nearly 100% was obtained. Increasing the dose of ionic liquid can enhance the acidity of the reaction system, thereby promoting the generation of more ROSs to accelerate the oxidation of DBT. Therefore, 0.2 g DIL was selected as the optimal dosage.

The effect of the H_2O_2 dosage on the sulfur removal capacity was investigated in this research. As shown in Fig. 5(b)—a dose of 0.5 and 1.0 mL resulted in a DBT removal rate of 87.4% and 100%, respectively. With a reaction time of 20 min, more ROSs can be generated to oxidize DBT as the amount of H_2O_2 increases. However, when a 1.5 mL dose of H_2O_2 was used, the DBT removal rate was 96.7% with a reaction time of 20 min. The slight decrease in the DBT removal rate was due to the large amount of water reducing the oxidant concentration, which resulted in a reduction in reactivity (Ali et al., 2009; Nie et al., 2014). Therefore, the optimal amount of H_2O_2 was determined to be 1.0 mL (O/S molar ratio = 43.5). Through experimental studies, it was found that reducing the amount of H_2O_2 (refers to decreasing O/S ratio) leads to a longer time required to achieve nearly 100% removal rate of DBT. For instance, when the H_2O_2 dosage is 1.0 mL (O/S = 43.5), a 100% removal rate of DBT can be achieved in 20 min. However, with a reduced H_2O_2 dosage of 0.5 mL (O/S = 21.75), the time needed to achieve a 99.1% removal rate extends to about 40 min. Lowering the H_2O_2 dosage to 0.25 mL (O/S = 10.8) increases the reaction time required for a 99.5% removal rate to approximately 60 min. In other words, a lower O/S typically requires a longer reaction time to reach the steady state. Regarding the safety concerns associated with using H_2O_2 as an oxidant, more future works are highly recommended by developing efficient oxidative desulfurization methods under low O/S ratio.

The effect of the AcOH dose used on the DBT removal rate was also investigated. Fig. 5(c) shows that the DBT removal only reaches 10.6% after 20 min, with an AcOH dose of 1 mL. When the dose of AcOH was increased to 2 mL, the DBT removal rate reached 100% after 20 min. This was because more AcOH can provide more PAA and other ROSs with H_2O_2 for the oxidation reaction of DBT. In addition, when the amount of acetic acid was increased to 3 mL, the time required for the desulfurization rate to reach 100% was also 20 min, and the reaction speed was not accelerated significantly. A high dose of AcOH does not change the equilibrium of the reversible reaction of AcOH and H_2O_2, therefore, the optimal dose of AcOH was determined to be 2 mL.

Fig. 5(d) shows the effect that the stirring rate has on the DBT removal rate. When the stirring rate is 0 r/min, the driving force for the mass transfer of DBT in the two phases is the difference in the concentration rate. Furthermore, DBT is insoluble in the water

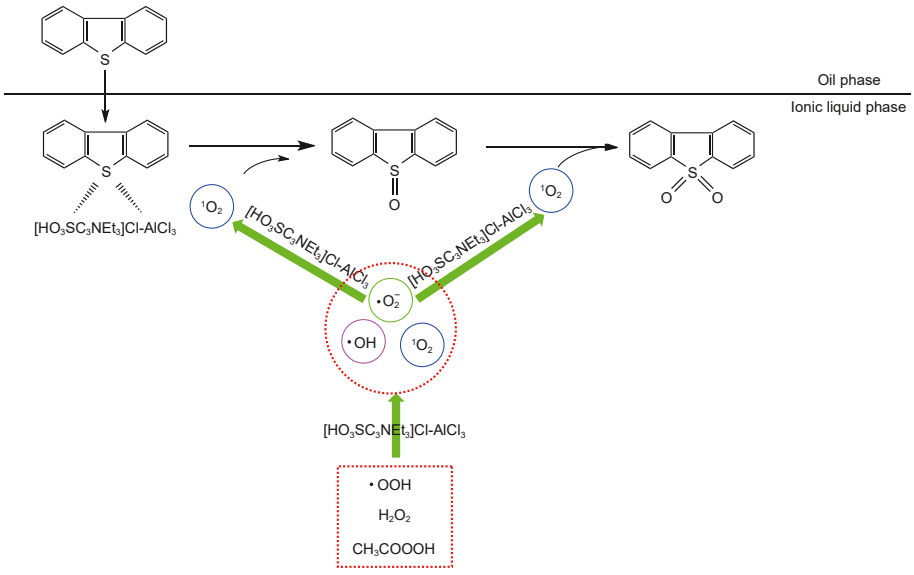

Fig. 4. Suggested process of DBT catalytic oxidation in the DIL-H_2O_2-AcOH reaction system.

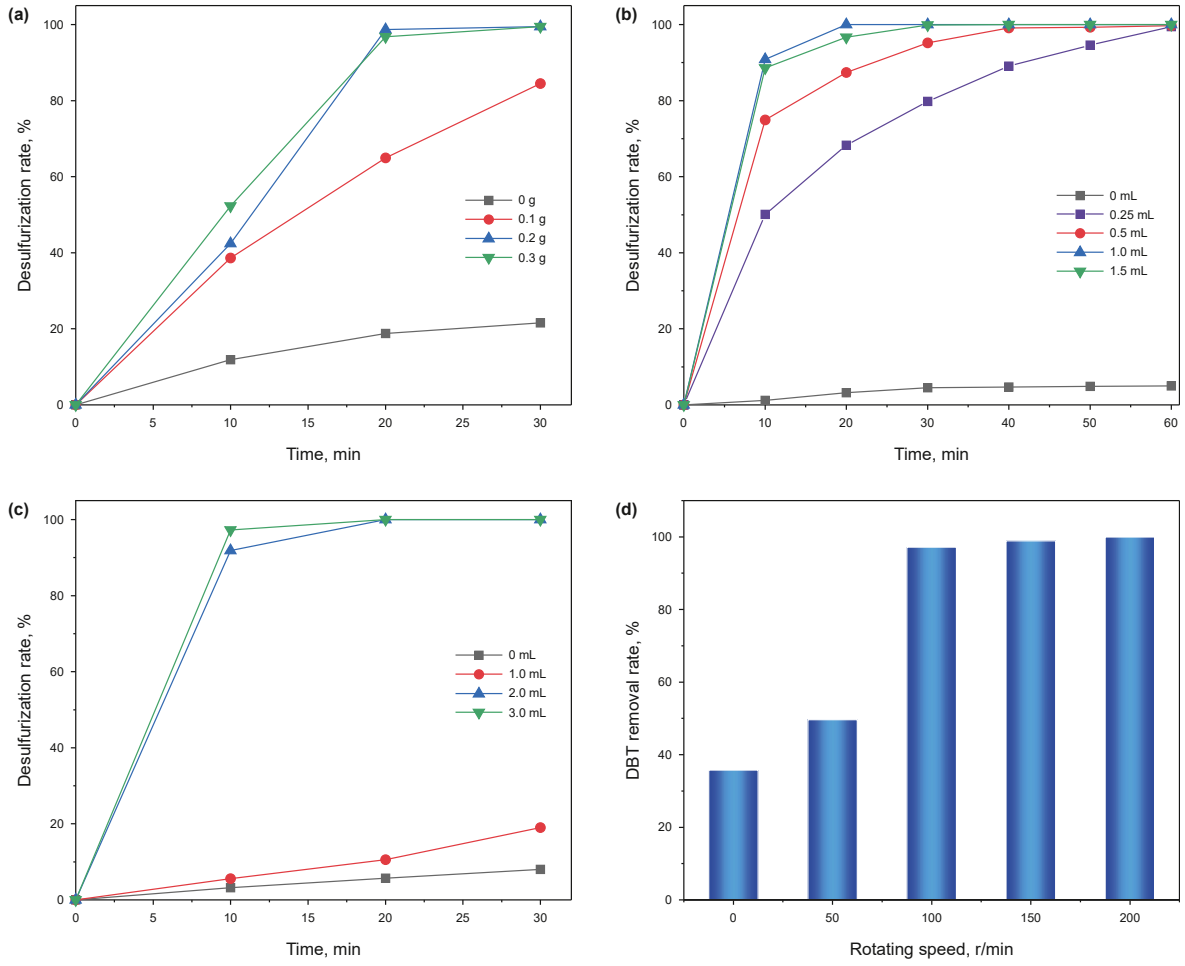

Fig. 5. **(a)** Effect of DIL dosage on DBT removal. **(b)** Effect of the amount of H_2O_2 on DBT removal rate. **(c)** Effect of AcOH dose on DBT removal rate. **(d)** Effect of stirring rate on DBT removal rate. Conditions: V (model oil: DBT (1000 ppm) in n-octane) = 10 mL; m(DIL) = 0.2 g for Fig. 5 (b)–(d); V (H_2O_2) = 1.0 mL for Fig. 5 (a), (c) and (d); V (AcOH) = 2.0 mL for Fig. 5 (a), (b) and (d); T = 55 °C; reaction time = 30–60 min; Stirring rate 200 r/min for Fig. 5 (a)–(c).

phase, so DBT in the oil phase cannot make adequate contact with the oxidants in the aqueous phase: only 35.7% of DBT removal efficiency is the result of free diffusion of DBT. When gradually increasing the stirring rate from 50 to 200 r/min, contact between DBT and ROSs and the catalyst improves significantly, which leads to a significant increase in DBT oxidation. When the stirring rate exceeds 200 r/min, the mass transfer diffusion limitations of reactants in different phases in the desulfurization system can be

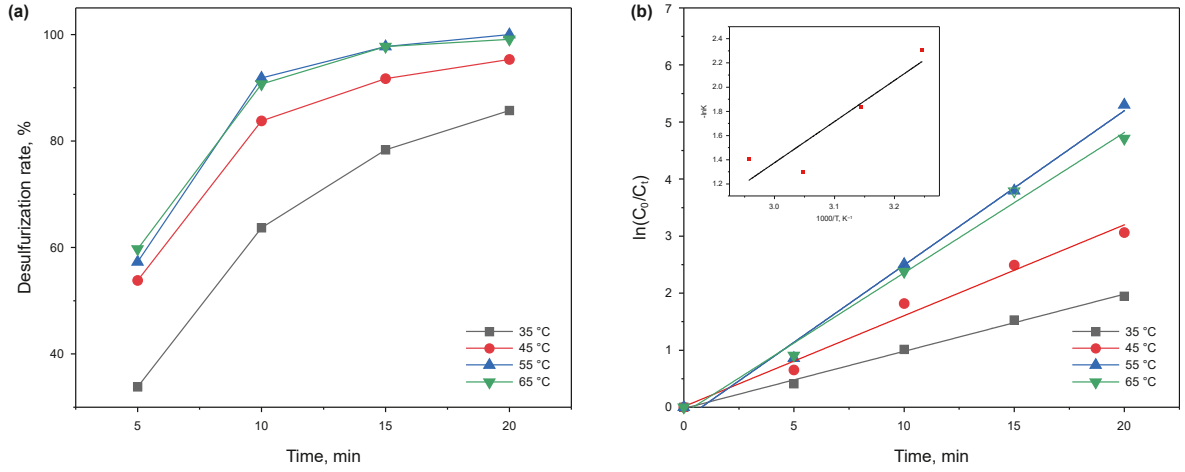

Fig. 6. **(a)** Effect of reaction temperatures on DBT removal with time on stream. **(b)** Time-course variation of ln (C_0/C_t) with different reaction temperatures. Conditions: m (DIL) = 0.2 g; V (model oil) = 10 mL; V (H_2O_2) = 1.0 mL; V (AcOH) = 2.0 mL; stirring rate = 200 r/min; DBT (1000 ppm) in n-octane.

eliminated (Liu et al., 2023d), and the effect of the stirring rate on the reaction rate is no longer significant. Therefore, the optimal stirring rate for this reaction system was determined to be 200 r/min.

Temperature has a significant effect on the desulfurization reaction and is also a critical factor in the reaction kinetics. Fig. 6(a) shows the DBT removal rate at different temperature levels. The rate of DBT removal from model oil increased along with a temperature increase from 35 to 65 °C. When the reaction time reached 20 min, the DBT removal efficiency reached 100% at temperature conditions of 55 and 65 °C. This is because increasing the reaction temperature is beneficial to the H_2O_2-AcOH system to produce peroxyacetic acid and ROSs, which can promote the oxidation reaction rate of DBT. However, at higher temperatures, the self-ineffective decomposition of H_2O_2 and PAA is accelerated (Collins et al., 1997; Lü et al., 2017), resulting in no further improvement in the desulfurization effect. Therefore, the optimal reaction temperature is 55 °C.

The effect of desulfurization when using various reaction temperatures was compared quantitatively. If the oxidation of DBT is treated as the pseudo-first-order reaction (Liu et al., 2023d), the equation of rate constant for the apparent consumption of DBT was employed as follows:

$$\ln(C_0 / C_t) = kt \tag{12}$$

The result of the time-course variation of ln (C_0/C_t) shown in Fig. 6(b), which exhibited the plotting ln (C_0/C_t) against reaction time t is a straight line. The fitted equations of ln(C_0/C_t) to time for DBT oxidation using different temperatures that were obtained using the least square method are shown in Table 3. In addition, according to the Arrhenius equation:

$$\ln k = -\mathrm{E_a}/RT + \ln k_0 \tag{13}$$

Using the least square method to fit ln k and 1/T, the apparent activation energy (E_a) and half-life are 36.8 kJ/mol and 260 s, respectively. The results indicate that the appropriate temperature is 55 °C.

3.5. Effect of sulfur content and oil volume on DBT removal

The removal rate of DBT in model oil with different sulfur content levels (50, 100, 500, 1000, 2000 and 4000 ppm) was investigated. Fig. 7(a) shows that the desulfurization rate of the ODS system for model oil with a DBT content below 1000 ppm reached 100% with a 20-min reaction. When the DBT content increased to 2000 and 4000 ppm, the desulfurization rate decreased to 96.7% and 91.2%, respectively. This result indicates that the desulfurization effect of the ODS system decreased for a sample with high sulfur content. The desulfurization effects of different doses of model oil (DBT content of 1000 ppm), including 5, 10, 15, and 20, were further investigated. Fig. 7(b) shows that the DBT removal rate can reach 100% with the 5 and 10 model oil; however, when the dose of model oil was 15 and 20 mL, the DBT removal rate decreased slightly to 98.6% and 95.7%, respectively, with the 20 min reaction time. These results indicate that although the sulfur concentration level remained constant at 1000 ppm, as the volume of the model oil increased, the absolute amount of DBT that needed to be oxidized increased with increasing the oil volume. At the same time, the increase in the volume of model oil can also lead to a decrease in the contact among the catalyst and the oxidant and the sulfur in the model oil. Therefore, to process a larger amount of model oil, the dose of oxidant and catalyst in the oxidation system should be increased.

Table 3
Fitted equation for desulfurization of DBT at different temperatures.

T, °C	Equation for fitting straight lines	R^2	K, min^{-1}
35	$\ln(C_0/C_t) = 0.1002t - 0.0214$	0.9962	0.1002
45	$\ln(C_0/C_t) = 0.1593t - 0.0124$	0.9850	0.1593
55	$\ln(C_0/C_t) = 0.2707t - 0.2148$	0.9926	0.2707
65	$\ln(C_0/C_t) = 0.2460t - 0.1035$	0.9928	0.2460

3.6. Optimization of oxidative desulfurization process conditions by RSM

According to the results obtained in Section 3.5, reaction time, reaction temperature and the ratio of AcOH/H_2O_2 are the tree core factors, which significantly affect the desulfurization rate; and the optimum conditions for DBT removal were: reaction time 20 min, reaction temperature 55 °C and H_2O_2/AcOH volume ratio 2 (1 mL H_2O_2, 2 mL AcOH). In this section, RSM was used to further optimize the experimental conditions of oxidative desulfurization (Dixit and Yadav, 2019; Shirley and Giauque, 1959). The reaction time, reaction temperature and H_2O_2/AcOH volume ratio of the DIL-ODS reaction system were marked as influencing factors X_1, X_2 and X_3, respectively. The desulfurization removal percentage was used as the response value, with the Box-Behnken model in Design-Expert software used to optimize the experimental conditions, and use graphics to display the relationship between various factor functions to determine the optimal conditions for experimental design. The experiments were divided into 17 groups. Experiments 1–12 were factorial experiments that were used to test the interaction between various factors. Experiments 13–17 were the core experiments that were used to calculate and evaluate experimental deviation. The coding level of each factor in the experimental design is shown in Table 4, and the experimental program and response surface analysis results are shown in Table 5.

The results of the optimization analysis are shown in Table 6. The $p < 0.0001$ of the model indicates that the quadratic regression model is significant. The linear relationship between response value Y and influencing factors X_1, X_2 and X_3 is obvious, and the regression model can be used to predict the desulfurization rate. The p-value in Table 6 indicates the significance level of the three factors in the established model. If the p-value is less than 0.05, it indicates that the influence is significant; if the p-value is greater than 0.05, it indicates that the influence of each factor in the model is not significant. For the results shown in Table 6, the p-value of the model is less than 0.05 this indicates that the quadratic equation model is significant, and the orthogonal test results and the mathematical model fit well. The optimization result inferred by the mathematical model is correct and useable.

The value of the correlation coefficient R^2 of the equation is 0.99. This indicates that most of the experiment data can be interpreted using this model and that the optimized experiment data obtained is reliable. Analysis of the F-value in Table 6 shows that the H_2O_2/AcOH volume ratio has the greatest influence on the response value among the three influencing factors, followed by the reaction temperature, and reaction time. By performing multiple regression on the desulfurization efficiency experimental data, the quadratic polynomial regression equation of each influencing factor on the desulfurization rate (Y) was obtained as follows:

$$Y = 100 + 2.01375X_1 + 1.725X_2 + 44.3463X_3 - 0.8375X_1X_2 - 1.68X_1X_3 - 0.2775X_2X_3 - 1.28{X_1}^2 - 2.2825{X_2}^2 - 43.39{X_3}^2$$

The three-dimensional (3-D) response surface and contour plots

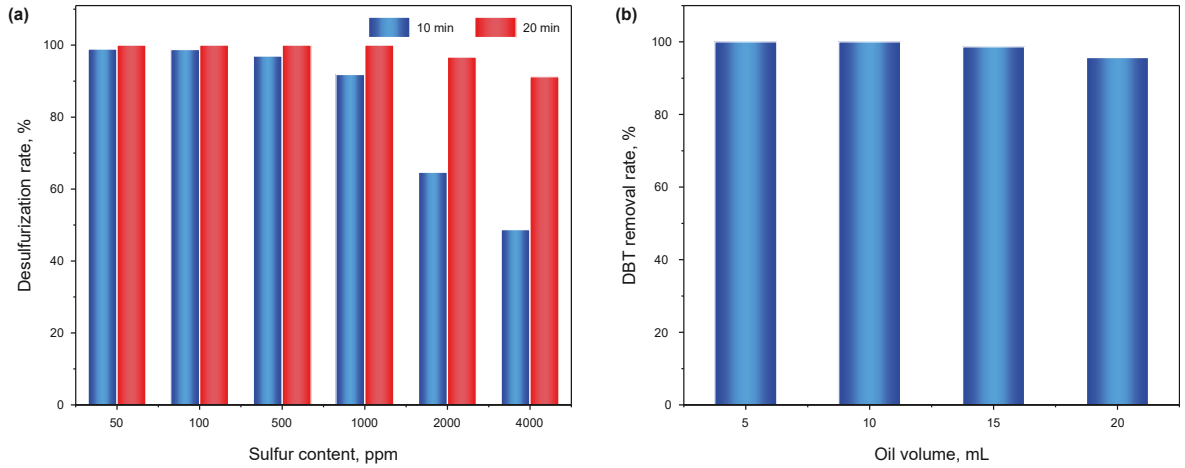

Fig. 7. Effect of **(a)** Sulfur concentration and **(b)** model oil volume on DBT removal. Conditions: m (DIL) = 0.2 g; V (H_2O_2) = 1.0 mL; V (AcOH) = 2.0 mL; T = 55 °C; reaction time = 20 min; stirring rate = 200 r/min; DBT (1000 ppm) in n-octane.

Table 4
Coding levels of various factors in the experimental design.

Factor	Variable	Range and level		
		−1	0	1
Reaction time, min	X_1	15	20	25
Reaction temperature, °C	X_2	45	55	65
AcOH/H_2O_2 volume ratio, mL/mL	X_3	1	2	3

Table 5
Experimental design and response values for the desulfurization of model oil.

Entry	Variable and level			Desulfurization rate, %	
	X_1	X_2	X_3	Experimental	Predicted
1	−1	1	0	97.73	96.99
2	0	−1	1	97.78	97.13
3	−1	0	1	98.72	99.24
4	0	1	−1	11.43	12.08
5	1	−1	0	96.82	97.56
6	1	1	0	99.47	99.34
7	−1	−1	0	91.73	91.86
8	−1	0	−1	7.3	7.39
9	1	0	−1	15.3	14.78
10	0	1	1	99.8	100.02
11	0	−1	−1	8.3	8.08
12	1	0	1	100	99.91
13	0	0	0	99.92	100.00
14	0	0	0	100	100.00
15	0	0	0	99.81	100.00
16	0	0	0	100	100.00
17	0	0	0	100	100.00

of the interaction between each of the three factors (reaction time (X_1), reaction temperature (X_2) and AcOH/H_2O_2 volume ratio (X_3)) obtained from the predicted model are shown in the supporting information (see Figs. S2, S3, and S4). The correlation between reaction time and AcOH/H_2O_2 volume ratio is shown in Fig. S2. The desulfurization rate increased with an increase in the AcOH/H_2O_2 volume ratio when the reaction time was kept constant. When the AcOH/H_2O_2 volume ratio was higher than 2, the desulfurization rate reached 100%, but it is meaningless to increase the volume ratio to increase the desulfurization rate. When the AcOH/H_2O_2 volume ratio is fixed, the desulfurization rate also increases with an increase in reaction time. The contour in Figs. S2–S4 indicates that the interaction between the reaction time and the AcOH/H_2O_2 volume ratio is significant, which is consistent with the results of the variance analysis.

Fig. S3 shows the correlation between the reaction time and reaction temperature. The desulfurization rate increased with an increase in reaction temperature at a fixed reaction time. The desulfurization rate reached 100% when the reaction temperature reached 55 °C. When the reaction temperature was fixed, the desulfurization rate also increased with an increase in reaction time. The contour shows that the interaction between reaction time and reaction temperature is significant, which is consistent with the results of the variance analysis.

Fig. S4 shows that the desulfurization rate is positively correlated with the AcOH/H_2O_2 volume ratio and reaction temperature by single-factor experiments. The 3D response surface indicates that, at a fixed AcOH/H_2O_2 volume ratio, the desulfurization rate still increased with an increase in the reaction temperature, but the contour line with a relatively large arc shows that the interaction between AcOH/H_2O_2 volume ratio and reaction temperature was not significant. This is consistent with the results of the variance analysis.

Based on the response surface and quadratic regression model analysis, and the effect that various factors have on the desulfurization rate when using [$HSO_3C_3NEt_3$]Cl-$AlCl_3$ catalyst, the optimum conditions were determined as follows: a reaction time of 21.8 min; a volume ratio of AcOH to H_2O_2 of 2.5; a reaction temperature of 57.8 °C. The predicted desulfurization rate can reach 109.2%.

Three experiments were performed using the optimum conditions using [$HSO_3C_3NEt_3$]Cl-$AlCl_3$ catalyst. The desulfurization rate was 100% in all instances. Additionally, parallel experiments were conducted using an AcOH/H_2O_2 volume ratio of 2 (2 mL AcOH, 1 mL H_2O_2), a reaction temperature of 55 °C and a reaction time of 20 min. A desulfurization rate of 100% was recorded, which is in good agreement with the predicted result. Thus, it is concluded that the model was reliable and the quadratic regression model truly reflects the effect that the three variables have on the desulfurization rate.

3.7. Desulfurization of different aromatic sulfurs and real diesel

The desulfurization effect of different aromatic sulfurs, including T, BT, 2-MBT, DBT and 4,6-DMDBT was estimated with the IL-H_2O_2-AcOH system under the same conditions. The results of removing different aromatic sulfur compounds in this system are

Table 6
Analysis of variance on response surface.

Source	Sum of squares	Degree of freedom	Mean square	F-Value	*p*-Value	Significance
Model	23809.37	9	2645.49	6973.14	<0.0001	a
X_1	32.44	1	32.44	85.51	<0.0001	a
X_2	23.80	1	23.80	62.75	<0.0001	a
X_3	15661.85	1	15661.85	41282.50	<0.0001	a
X_1X_2	2.81	1	2.81	7.40	0.0298	a
X_1X_3	11.29	1	11.29	29.76	0.0010	a
X_2X_3	0.3080	1	0.3080	0.8119	0.3975	
X_1^2	6.90	1	6.90	18.18	0.0037	a
X_2^2	21.94	1	21.94	57.82	0.0001	a
X_3^2	7927.12	1	7927.12	20894.83	<0.0001	a
Residual	2.66	7	0.3794			
Lack of fit	2.66	3	0.8852			
Pure error	0.0000	4	0.0000			
Cor. total	23812.03	16				

[a] means highly significant.

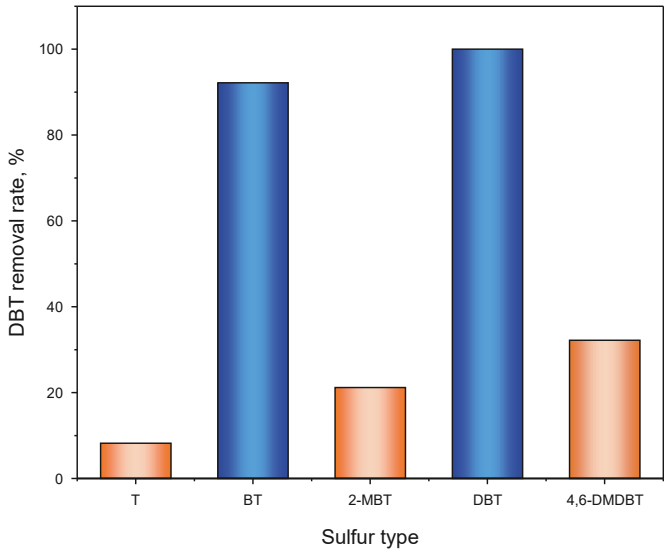

Fig. 8. Desulfurization effect of different S-compounds. Conditions: m (IL) = 0.2 g; V (H_2O_2) = 1.0 mL; V (AcOH) = 2.0 mL; T = 55 °C; reaction time = 20 min; stirring rate = 200 r/min; S-compounds (1000 ppm) in n-octane.

shown in Fig. 8. The desulfurization rate of T model oil, BT model oil, 2-MBT model oil, DBT model oil and 4,6-DMDBT model oil is 8.2%, 92.1%, 21.2%, 100% and 32.2%, respectively, after 20 min. So, sulfur removal capacity for different aromatic sulfurs decreased in the order of DBT > BT ≫ 4,6-DMDBT > 2-MBT > T.

In the studies conducted by Otsuki et al. (2000) and Shiraishi et al. (2002), it was reported that the oxidation rate of aromatic sulfides increased with the enhancement of electron density on the sulfur atoms (4,6-DMDBT > DBT > 2-MBT > BT > T). Additionally, the electron density of DBTs and BTs increased with an increase in the number of alkyl substituents on the carbon atoms, which means that DBTs and BTs with higher carbon alkyl substituents are more susceptible to oxidation. However, in this study, 4,6-DMDBT and 2-MBT (which have a higher electron density on the sulfur atoms) exhibited a lower desulfurization rate of 32.2% and 21.2%, respectively, compared to DBT and BT. This does not conform with the previously observed relationship between electron density and oxidation rate. Therefore, the reasons for the low desulfurization efficiency of 4,6-DMDBT and 2-MBT model oils had to be investigated in this study.

The gas chromatography (GC) of 2-MBT and 4,6-DMDBT model oils before and after desulfurization are shown in Fig. 9. A comparison of the GC chromatogram of 2-MBT model oil before (Fig. 9(a)) and after (Fig. 9(b)) desulfurization reveals a significant reduction of the signal of 2-MBT peak. However, the oxidation products after desulfurization, 2-methylbenzothiophene sulfoxide (2-MBTO) and 2-methylbenzothiophene sulfone (2-MBTO$_2$), are accompanied by two signal peaks with longer retention time. This suggests that the oxidation product of 2-MBT remained at the oil phase due to the poor solubility in water, only a small part had entered the water phase, resulting in a reduced desulfurization rate.

In the GC chromatogram of 4,6-DMDBT model oil before (Fig. 9(c)) and after (Fig. 9(d)) desulfurization, a slight reduction in the signal peak is observed after the reaction, indicating the challenging oxidation of 4,6-DMDBT. Similarly, two weak signal peaks in the oxidation products, 4,6-dimethyldibenzothiophene sulfoxide (4,6-DMDBTO) and 4,6-dimethyldibenzothiophene sulfone (4,6-DMDBTO$_2$), appear at a longer retention time, which indicates that little 4,6-DMDBTO and 4,6-DMDBTO$_2$ remains in the oil phase.

In summary, the low desulfurization efficiency of 4,6-DMDBT and 2-MBT model oils could be attributed to the steric hindrance introduced by the methyl groups on the aromatic ring, which makes it difficult for the sulfur atom in aromatic sulfides to encounter active oxygen species. This then reduces their susceptibility to oxidation. Additionally, the high hydrophobicity of the sulfone oxidation products of 4,6-DMDBT and 2-MBT led to their retention in the oil phase, which further reduced the desulfurization rate. This finding ties in well with the results reported by Li et al. (2016), Zhao et al. (2017) and Wang et al. (2020b).

This IL-ODS system was also applied to actual diesel with a sulfur content of 726 ppm. Table 7 shows that the lower-phase displays a rather low extractability (9.3%) of sulfur compounds by only extraction. When using the DIL-ODS desulfurization system, the sulfur removal rate can reach 68.6% and 79.8% at 20 and 40 min, respectively. In this DIL-ODS system, in addition to the unique mechanism of DIL mentioned above, the good desulfurization performance of the DIL may also be attributed to the ability of the quaternary ammonium cations ($[HSO_3C_3NEt_3]^+$) in the DIL to form metastable emulsion droplets in actual diesel with an aqueous H_2O_2 solution, which is also beneficial to the oxidation of sulfides (Jiang et al., 2011).

The S-compounds in the actual diesel contain T, BT and DBT and their thioalkyl-substituted derivatives, and other impurities. Therefore, the desulfurization effect of actual diesel is lower than that of model oil. The GC chromatogram of actual diesel (Fig. 10) before and after desulfurization indicates that most of the 2-MBT, DBT, 4,6-DMDBT and their derivatives, can be oxidatively removed. However, T and Ts, as well as a portion of BT are difficult to oxidize and remove.

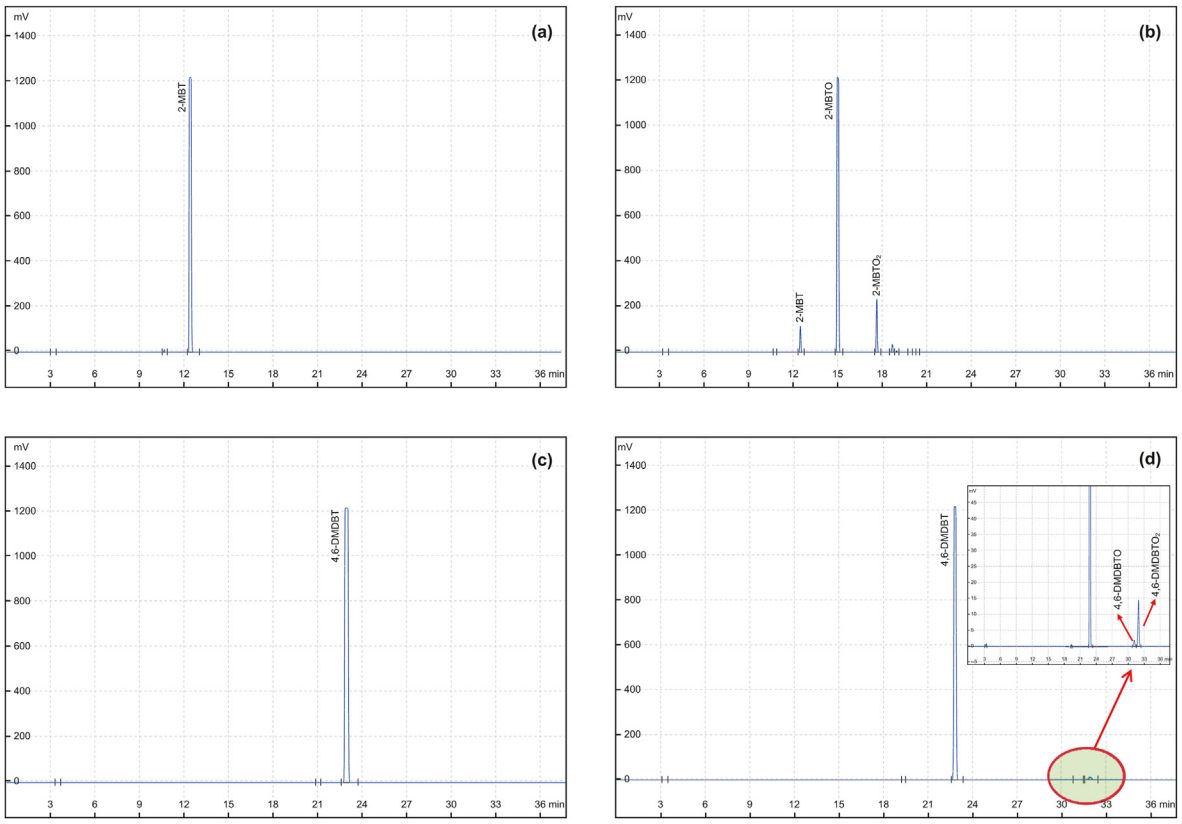

Fig. 9. GC chromatogram of 2-MDBT model oil **(a)** before and **(b)** after desulfurization and 4,6-DMDBT model oil **(c)** before and **(d)** after desulfurization. Conditions: m (IL) = 0.2 g; V (H_2O_2) = 1.0 mL; V (AcOH) = 2.0 mL; T = 55 °C; reaction time = 20 min; stirring rate = 200 r/min; S-compounds (1000 ppm) in n-octane.

Table 7
Desulfurization effect of actual diesel.

Entry	Sulfur content, ppm	DBT removal, %	Reaction time, min	Yield of oil, %
Actual diesel oil	726	–	–	–
Only by extraction	658.5	9.3	–	>99
IL-ODS system	227.9	68.6	20	>99
	146.2	79.8	40	>99

Conditions: m (IL) = 0.2 g; V (H_2O_2) = 1.0 mL; V (AcOH) = 2.0 mL; T = 55 °C; stirring rate = 200 r/min; S-compounds (726 ppm) in diesel.

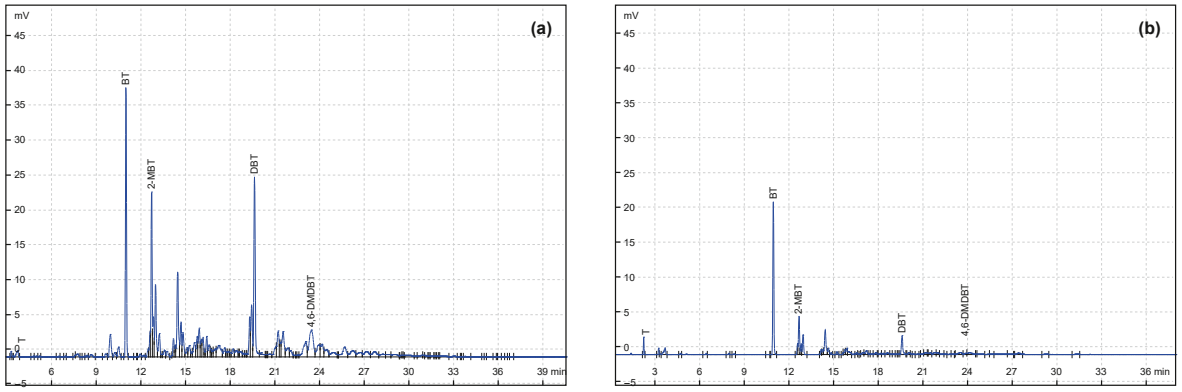

Fig. 10. The GC of actual diesel before **(a)** and after **(b)** desulfurization (reaction time = 40 min).

3.8. Recycling of DIL

The recycling performance of DIL is important due to expectations of its large-scale industrial applications. In this study, the $[HSO_3C_3NEt_3]Cl$-$AlCl_3$ is immiscible with the oil phase, therefore, after each run, the oil phase (upper layer) was separated by means of decantation after the reaction. Subsequently, the oxidation product $DBTO_2$ was filtered out from the aqueous phase (lower

layer). Finally, the lower layer (aqueous layer, containing water, H_2O_2, AcOH, and $[HSO_3C_3NEt_3]Cl$-$AlCl_3$) was heated at 80 °C under reduced pressure for 25 min to remove water, H_2O_2 and AcOH. The $[HSO_3C_3NEt_3]Cl$-$AlCl_3$ was retained in the flask. And the same amount of fresh H_2O_2 and AcOH as previous were added to the reaction system for the next run. There is a common problem of ionic liquid loss during the recovery process of ionic liquids. At the same time, because the amount of $[HSO_3C_3NEt_3]Cl$-$AlCl_3$ used in this experiment is very small, it also makes the recovery of ionic liquids difficult. Therefore, the loss during the recovery process of ionic liquid is the main reason for the decline in desulfurization performance during recycling, and the DBT removal rate dropped to 78.2% in 4 runs, as shown in Fig. 11. Even so, the recycling results indicates that the addition of a tiny amount of $[HSO_3C_3NEt_3]Cl$-$AlCl_3$ can achieve quite impressive desulfurization performance. This is a notable aspect of this experiment. The solubility of $DBTO_2$ as the main oxidation product of DBT was measured. The results show that the solubility of $DBTO_2$ reaches 0.231×10^{-4} mol (0.005 g) in the aqueous phase, which corresponds to 0.000739 g sulfur in the lower layer, i.e. 739 ppm $DBTO_2$ calculated by S-content can be dissolved in the lower-phase. This value indicated the limited solubility of $DBTO_2$ in the aqueous phase. White precipitant was obtained during recycling cycles of desulfurization.

4. Conclusion

In this study, four types of DILs: $[HSO_3C_3NEt_3]Cl$-$AlCl_3$, $HSO_3C_3NEt_3]Cl$-$ZnCl_2$, $[HSO_3C_3NEt_3]Cl$-$CuCl_2$ and $[HSO_3C_3NEt_3]Cl$-$FeCl_3$ were prepared, and these served as the catalysts and extractants for ODS of model oil and real diesel. However, The results indicated that $[HSO_3C_3NEt_3]Cl$-$CuCl_2$ and $[HSO_3C_3NEt_3]Cl$-$FeCl_3$ exhibit a negligible desulfurization effect due to their rapid decomposition of H_2O_2. In contrast, $[HSO_3C_3NEt_3]Cl$-$AlCl_3$ and $HSO_3C_3NEt_3]Cl$-$ZnCl_2$ demonstrated a remarkably good catalytic oxidative desulfurization performance. Under mild conditions (55 °C, 20 min), a mere 0.2 g of these catalysts resulted in DBT removal rates of 100% and 91.2%, respectively, in 10 mL model oil. When using $[HSO_3C_3NEt_3]Cl$-$AlCl_3$ as the representative sample, a mechanistic study revealed that the DIL, which is characterized by a weak Lewis acidic cation and a strong Lewis acidic anion, induces the dismutation of superoxide anions, which may lead to the generation of $^1O_2$. The oxidation of DBT was primarily attributed to a non-radical mechanism dominated by $^1O_2$. Additionally, the structural characteristics of the DIL catalyst facilitated the efficient and rapid mass transfer of DBT. The DIL also performed a surfactant-like function and promoted contact between the reaction substrates. Due to steric hindrance and hydrophobicity, the DIL-ODS system suffered from some limitations in oxidative desulfurization of alkyl-substituted aromatic sulfurs, such as 2-MBT and 4,6-DMDBT. Furthermore, when keeping other conditions constant, but extending the reaction time to 40 min, a desulfurization efficiency of 79.8% was recorded for actual diesel. The DIL-ODS system can be recycled 4 times without a noticeable decrease in activity. This work provides new insight into ODS and is an effective means of using DILs for deep desulfurization of fuel oil. It also suggests a promising avenue for industrial application of oxidative desulfurization technology.

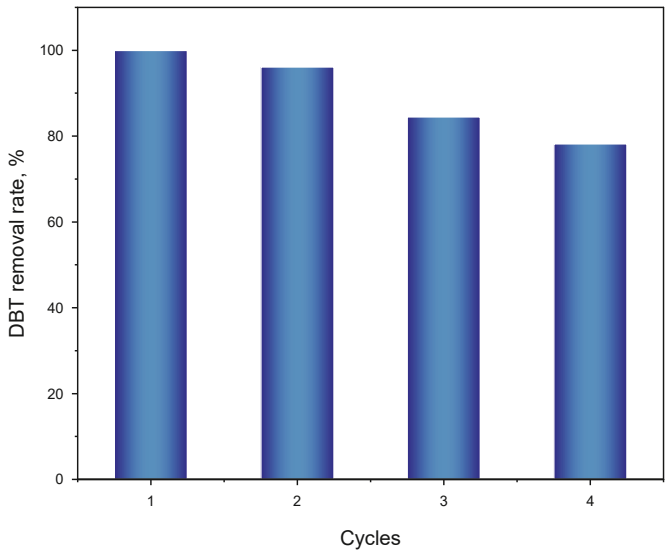

Fig. 11. Recycling of $[HSO_3C_3NEt_3]Cl$-$AlCl_3$ on removal of DBT in model oil. Conditions used with all cycles: m (DIL) = 0.2 g; V (H_2O_2) = 1.0 mL; V (AcOH) = 2.0 mL; T = 55 °C; reaction time = 20 min; stirring rate = 200 r/min; DBT (1000 ppm) in n-octane.

CRediT authorship contribution statement

Ran Liu: Writing – original draft, Software, Methodology, Investigation, Formal analysis, Conceptualization. **Chang Wang:** Visualization, Software, Data curation. **Qiang Yang:** Visualization, Formal analysis, Data curation. **Jing-Ran Yang:** Visualization, Investigation, Data curation. **Chen Liu:** Investigation, Data curation. **Liberty Mguni:** Formal analysis, Data curation. **Xin-Ying Liu:** Writing – review & editing, Supervision, Funding acquisition, Conceptualization. **Ya-Li Yao:** Writing – review & editing, Supervision, Resources, Conceptualization. **Fa-Tang Li:** Writing – review & editing, Supervision, Funding acquisition, Conceptualization.

Declaration of competing interest

The authors declare that they have no known competing financial interests or personal relationships that could have appeared to influence the work reported in this paper.

Acknowledgements

The authors are grateful for the financial support provided by South Africa National Research Foundation (UID 95983, 113648, 137947) and Foundation for Innovative Research Groups of the Natural Science Foundation of Hebei Province (no. B2021208005).

Appendix A. Supplementary data

Supplementary data to this article can be found online at https://doi.org/10.1016/j.petsci.2024.07.012.

References

Aghaei, A., Sobati, M.A., 2022. Extraction of sulfur compounds from middle distillate fuels using ionic liquids and deep eutectic solvents: a critical review. Fuel 310, 122279. https://doi.org/10.1016/j.fuel.2021.122279.

Ali, S.H., Hamad, D.M., Albusairi, B.H., Fahim, M.A., 2009. Removal of dibenzothiophenes from fuels by oxy-desulfurization. Energy Fuel. 23 (12), 5986–5994. https://doi.org/10.1021/ef900683d.

Ban, L.L., Liu, P., Ma, C.H., Dai, B., 2013. Deep extractive desulfurization of diesel fuels by $FeCl_3$/ionic liquids. Chinese Chem. Lett. 24 (8), 755–758. https://doi.org/10.1016/j.cclet.2013.04.031.

Bhasarkar, J.B., Chakma, S., Moholkar, V.S., 2013. Mechanistic features of oxidative desulfurization using sono-fenton-peracetic acid (ultrasound/Fe^{2+}-CH_3COOH-H_2O_2) system. Ind. Eng. Chem. Res. 52 (26), 9038–9047. https://doi.org/10.1021/ie400879j.

Bhutto, A.W., Abro, R., Gao, S., Abbas, T., Chen, X., Yu, G., 2016. Oxidative desulfurization of fuel oils using ionic liquids: a review. J. Taiwan Inst. Chem. Eng. 62, 84–97. https://doi.org/10.1016/j.jtice.2016.01.014.

Boshagh, F., Rahmani, M., Zhu, W., 2022b. Recent advances and challenges in developing technological methods assisting oxidative desulfurization of liquid

fuels: a review. Energy Fuel. 36 (21), 12961–12985. https://doi.org/10.1021/acs.energyfuels.2c03218.
Boshagh, F., Rahmani, M., Rostami, K., Yousefifar, M., 2022a. Key factors affecting the development of oxidative desulfurization of liquid fuels: a critical review. Energy Fuel. 36 (1), 98–132. https://doi.org/10.1021/acs.energyfuels.1c03396.
Bösmann, A., Datsevich, L., Jess, A., Lauter, A., Schmitz, C., Wasserscheid, P., 2001. Deep desulfurization of diesel fuel by extraction with ionic liquids. Chem. Commun. 23, 2494–2495. https://doi.org/10.1039/b108411a.
Chen, X., Song, D., Asumana, C., Yu, G., 2012. Deep oxidative desulfurization of diesel fuels by Lewis acidic ionic liquids based on 1-n-butyl-3-methylimidazolium metal chloride. J. Mol. Catal. Chem. 359, 8–13. https://doi.org/10.1016/j.molcata.2012.03.014.
Chen, X., Yuan, S., Abdeltawab, A.A., Al-Deyab, S.S., Zhang, J., Yu, L., et al., 2014. Extractive desulfurization and denitrogenation of fuels using functional acidic ionic liquids. Sep. Purif. Technol. 133, 187–193. https://doi.org/10.1016/j.seppur.2014.06.031.
Collins, F.M., Lucy, A.R., Sharp, C., 1997. Oxidative desulphurisation of oils via hydrogen peroxide and heteropolyanion catalysis. J. Mol. Catal. Chem. 117 (1–3), 397–403. https://doi.org/10.1016/S1381-1169(96)00251-8.
Desai, K., Dharaskar, S., Pandya, J., Shinde, S., Vakharia, V., 2022. Experimental investigation and validation of ultrasound-assisted extractive/oxidative desulfurization of oil using environmentally benign ionic liquid. Process Saf. Environ. Prot. 166, 512–523. https://doi.org/10.1016/j.psep.2022.08.029.
Dharaskar, S., Desai, K., Tadi, K.K., Sillanpää, M., 2021. Synthesis, Characterization and application of trihexyl (tetradecyl) phosphonium bromide as a promising solvent for sulfur extraction from liquid fuels. Ind. Eng. Chem. Res. 60 (46), 16769–16779. https://doi.org/10.1021/acs.iecr.1c02169.
Dharaskar, S., Sillanpaa, M., 2018. Synthesis, characterization, and application of trihexyl(tetradecyl)phosphonium chloride as promising solvent for extractive desulfurization of liquid fuel. Chem. Eng. Res. Des. 133, 388–397. https://doi.org/10.1016/j.cherd.2018.03.016.
Dharaskar, S.A., Wasewar, K.L., Varma, M.N., Shende, D.Z., 2013. Extractive deep desulfurization of liquid fuels using Lewis-Based ionic liquids. J. Energy 2013, 1–4. https://doi.org/10.1155/2013/581723.
Dharaskar, S.A., Wasewar, K.L., Varma, M.N., Shende, D.Z., 2015. $FeCl_3$ based imidazolium ionic liquids as novel solvents for extractive-oxidative desulfurization of liquid fuels. J. Solution Chem. 44 (3–4), 652–668. https://doi.org/10.1007/s10953-015-0310-8.
Dixit, S., Yadav, V.L., 2019. Optimization of polyethylene/polypropylene/alkali modified wheat straw composites for packaging application using RSM. J. Clean. Prod. 240, 118228. https://doi.org/10.1016/j.jclepro.2019.118228.
Eugene, A.J., Guzman, M.I., 2019. Production of singlet oxygen ($^1O_2$) during the photochemistry of aqueous pyruvic acid: the effects of pH and photon flux under steady-state O_2(aq) concentration. Environ. Sci. Technol. 53 (21), 12425–12432. https://doi.org/10.1021/acs.est.9b03742.
Ganiyu, S.A., Lateef, S.A., 2021. Review of adsorptive desulfurization process: Overview of the non-carbonaceous materials, mechanism and synthesis strategies. Fuel 294, 120273. https://doi.org/10.1016/j.fuel.2021.120273.
Ge, J., Zhou, Y., Yang, Y., Xue, M., 2011. Catalytic oxidative desulfurization of gasoline using ionic liquid emulsion system. Ind. Eng. Chem. Res. 50 (24), 13686–13692. https://doi.org/10.1021/ie201325e.
Gui, J., Liu, D., Sun, Z., Liu, D., Min, D., Song, B., et al., 2010. Deep oxidative desulfurization with task-specific ionic liquids: an experimental and computational study. J. Mol. Catal. Chem. 331 (1–2), 64–70. https://doi.org/10.1016/j.molcata.2010.08.003.
Hao, Y., Hao, Y.J., Ren, J., Wu, B., Wang, X.J., Zhao, D., et al., 2019. Extractive/catalytic oxidative mechanisms over [Hnmp]Cl:X $FeCl_3$ ionic liquids towards the desulfurization of model oils. New J. Chem. 43 (20), 7725–7732. https://doi.org/10.1039/c9nj00691e.
Haruna, A., Merican, Z.M.A., Musa, S.G., 2022. Recent advances in catalytic oxidative desulfurization of fuel oil – a review. J. Ind. Eng. Chem. 112, 20–36. https://doi.org/10.1016/j.jiec.2022.05.023.
Hodges, B.C., Cates, E.L., Kim, J.H., 2018. Challenges and prospects of advanced oxidation water treatment processes using catalytic nanomaterials. Nat. Nanotechnol. 13 (8), 642–650. https://doi.org/10.1038/s41565-018-0216-x.
Huang, C.P., Chen, B.H., Zhang, J., Liu, Z.C., Li, Y.X., 2004. Desulfurization of gasoline by extraction with new ionic liquids. Energy Fuel. 18, 1862–1864. https://doi.org/10.1021/ef049879k.
Ji, J., Wang, Z., Xu, Q., Zhu, Q., Xing, M., 2023. In situ H_2O_2 Generation and corresponding pollutant removal applications: a review. Chem.-A Eur. J. 29 (24), e202203921. https://doi.org/10.1002/chem.202203921.
Ji, J., Yan, Q., Yin, P., Mine, S., Matsuoka, M., Xing, M., 2021. Defects on CoS_2−x: tuning redox reactions for sustainable degradation of organic pollutants. Angew. Chemie - Int. Ed. 60 (6), 2903–2908. https://doi.org/10.1002/anie.202013015.
Jiang, Z., Lü, H., Zhang, Y., Li, C., 2011. Oxidative desulfurization of fuel oils. Chinese J. Catal. 32 (5), 707–715. https://doi.org/10.1016/S1872-2067(10)60246-X.
Khan, A.U., 1977. Theory of electron transfer generation and quenching of singlet oxygen [1Σg+ and 1Δg] by superoxide anion. the role of water in the dismutation of O_2. J. Am. Chem. Soc. 99 (2), 370–371. https://doi.org/10.1021/ja00444a010.
Konovalova, T.A., Lawrence, J., Kispert, L.D., 2004. Generation of superoxide anion and most likely singlet oxygen in irradiated TiO_2 nanoparticles modified by carotenoids. J. Photochem. Photobiol. Chem. 162 (1), 1–8. https://doi.org/10.1016/S1010-6030(03)00313-7.
Li, F.T., Kou, C.G., Sun, Z.M., Hao, Y.J., Liu, R.H., Zhao, D.S., 2012. Deep extractive and oxidative desulfurization of dibenzothiophene with $C_5H_9NO{\cdot}SnCl_2$ coordinated ionic liquid. J. Hazard Mater. 205–206, 164–170. https://doi.org/10.1016/j.jhazmat.2011.12.054.
Li, F.T., Liu, R.H., Wen, J.H., Zhao, D.S., Sun, Z.M., Liu, Y., 2009. Desulfurization of dibenzothiophene by chemical oxidation and solvent extraction with $Me_3NCH_2C_6H_5Cl{\cdot}2ZnCl_2$ ionic liquid. Green Chem. 11 (6), 883–888. https://doi.org/10.1039/b815575e.
Li, F.T., Liu, Y., Sun, Z.M., Chen, L.J., Zhao, D.S., Liu, R.H., et al., 2010. Deep extractive desulfurization of gasoline with $xEt_3NHCl{\cdot}FeCl_3$ ionic liquids. Energy Fuel. 24 (8), 4285–4289. https://doi.org/10.1021/ef100408h.
Li, F.T., Wu, B., Liu, R.H., Wang, X.J., Chen, L.J., Zhao, D.S., 2015a. An inexpensive N-methyl-2-pyrrolidone-based ionic liquid as efficient extractant and catalyst for desulfurization of dibenzothiophene. Chem. Eng. J. 274, 192–199. https://doi.org/10.1016/j.cej.2015.04.027.
Li, H., Chang, Y., Zhu, W., Jiang, W., Zhang, M., Xia, J., et al., 2015b. A DFT study of the extractive desulfurization mechanism by $[BMIM]^+[AlCl_4]^-$ ionic liquid. J. Phys. Chem. B 119 (19), 5995–6009. https://doi.org/10.1021/acs.jpcb.5b00516.
Li, H., Zhang, B., Jiang, W., Zhu, W., Zhang, M., Wang, C., et al., 2019. A comparative study of the extractive desulfurization mechanism by Cu(II) and Zn-based imidazolium ionic liquids. Green Energy Environ. 4 (1), 38–48. https://doi.org/10.1016/j.gee.2017.10.003.
Li, H., Zhu, W., Zhu, S., Xia, J., Chang, Y., Jiang, W., et al., 2016. The selectivity for sulfur removal from oils: an insight from conceptual density functional theory. AIChE J. 62 (6), 2087–2100. https://doi.org/10.1002/aic.15161.
Li, Z., Xu, J., Li, D., Li, C., 2015c. Extraction process of sulfur compounds from fuels with protic ionic liquids. RSC Adv. 5 (21), 15892–15897. https://doi.org/10.1039/C4RA16186F.
Ling, C., Liu, X., Li, H., Wang, X., Gu, H., Wei, K., et al., 2022. Atomic-layered Cu_5 nanoclusters on FeS_2 with dual catalytic sites for efficient and selective H_2O_2 activation. Angew. Chemie-Int. Ed. 61 (21), e202200670. https://doi.org/10.1002/anie.202200670.
Liu, F., Yu, J., Qazi, A.B., Zhang, L., Liu, X., 2021. Metal-based ionic liquids in oxidative desulfurization: a critical review. Environ. Sci. Technol. 55 (3), 1419–1435. https://doi.org/10.1021/acs.est.0c05855.
Liu, J., Deng, C., Liu, X., Shao, S., Zheng, P., Chen, L., et al., 2023d. Single Mo atoms stabilized on high-entropy perovskite oxide: a frontier for aerobic oxidative desulfurization. Inorg. Chem. 62 (28), 11044–11055. https://doi.org/10.1021/acs.inorgchem.3c01085.
Liu, J., Liu, X., Yan, R., Jia, L., Cheng, H., Liu, H., et al., 2023b. Active phase morphology engineering of $NiMo/Al_2O_3$ through La introduction for boosting hydrodesulfurization of 4,6-DMDBT. Petrol. Sci. 20 (2), 1231–1237. https://doi.org/10.1016/j.petsci.2022.09.023.
Liu, J., Zhang, L., Zhu, J., Cheng, H., Hua, M., Liu, H., et al., 2023c. Size-dependent surface electronic structure of V_2O_5/TiO_2 for ultra-deep aerobic oxidative desulfurization of diesel. Chem. Eng. Sci. 275, 118749. https://doi.org/10.1016/j.ces.2023.118749.
Liu, J., Zhu, J., Zhu, J., Xu, J., Liu, H., Hua, M., et al., 2023a. One-pot three-dimensional printing of a hierarchical $NiMo/Al_2O_3$ monolithic catalyst for 4,6-dimethyldibenzothiophene hydrodesulfurization. ACS Appl. Mater. Interfaces 15 (28), 33593–33604. https://doi.org/10.1021/acsami.3c05620.
Liu, R., Zhang, J., Xu, Z., Zhao, D., Sun, S., 2018. Visible light photocatalytic oxidative desulfurization using Ti-MCM-41-loaded iron phthalocyanine combined with ionic liquid extraction. J. Mater. Sci. 53 (7), 4927–4938. https://doi.org/10.1007/s10853-017-1954-0.
Lo, W.H., Yang, H.Y., Wei, G.T., 2003. One-pot desulfurization of light oils by chemical oxidation and solvent extraction with room temperature ionic liquids. Green Chem. 5 (5), 639–642. https://doi.org/10.1039/b305993f.
Lü, H., Li, P., Liu, Y., Hao, L., Ren, W., Zhu, W., et al., 2017. Synthesis of a hybrid Anderson-type polyoxometalate in deep eutectic solvents (DESs) for deep desulphurization of model diesel in ionic liquids (ILs). Chem. Eng. J. 313, 1004–1009. https://doi.org/10.1016/j.cej.2016.10.140.
Lu, L., Cheng, S., Gao, J., Gao, G., He, M.Y., 2007. Deep oxidative desulfurization of fuels catalyzed by ionic liquid in the presence of H_2O_2. Energy Fuel. 21 (1), 383–384. https://doi.org/10.1021/ef060345o.
Luo, J., Yan, M., Ji, H., Mu, L., Huang, Y., Zhu, L., et al., 2022. Three-dimensional Ce-MOFs-derived Ce@C-BN nanobundles for adsorptive desulfurization. Appl. Surf. Sci. 590, 152926. https://doi.org/10.1016/j.apsusc.2022.152926.
Malolan, R., Gopinath, K.P., Vo, D.V.N., Jayaraman, R.S., Adithya, S., Ajay, P.S., Arun, J., 2021. Green ionic liquids and deep eutectic solvents for desulphurization, denitrification, biomass, biodiesel, bioethanol and hydrogen fuels: a review. Environ. Chem. Lett. 19 (2), 1001–1023. https://doi.org/10.1007/s10311-020-01113-7.
Mourad, E., Petit, Y.K., Spezia, R., Samojlov, A., Summa, F.F., Prehal, C., et al., 2019. Singlet oxygen from cation driven superoxide disproportionation and consequences for aprotic metal-O_2 batteries. Energy Environ. Sci. 12 (8), 2559–2568. https://doi.org/10.1039/c9ee01453e.
Nie, Y., Dong, Y., Bai, L., Dong, H., Zhang, X., 2013. Fast oxidative desulfurization of fuel oil using dialkylpyridinium tetrachloroferrates ionic liquids. Fuel 103, 997–1002. https://doi.org/10.1016/j.fuel.2012.07.071.
Nie, Y., Gong, X., Gao, H., Zhang, X., Zhang, S., 2014. Simultaneous desulfurization and denitrogen of liquid fuels using two functionalized group ionic liquids. Sci. China Chem. 57 (12), 1766–1773. https://doi.org/10.1007/s11426-014-5164-1.
Nie, Y., Li, C., Sun, A., Meng, H., Wang, Z., 2006. Extractive desulfurization of gasoline using imidazolium-based phosphoric ionic liquids. Energy Fuel. 20 (5),

2083–2087. https://doi.org/10.1021/ef060170i.
Otsuki, S., Nonaka, T., Takashima, N., Qian, W., Ishihara, A., Imai, T., Kabe, T., 2000. Oxidative desulfurization of light gas oil and vacuum gas oil by oxidation and solvent extraction. Energy Fuel. 14 (6), 1232–1239. https://doi.org/10.1021/ef000096i.
Raj, J.J., Magaret, S., Pranesh, M., Lethesh, K.C., Devi, W.C., Mutalib, M.I.A., 2019. Dual functionalized imidazolium ionic liquids as a green solvent for extractive desulfurization of fuel oil: Toxicology and mechanistic studies. J. Clean. Prod. 213, 989–998. https://doi.org/10.1016/j.jclepro.2018.12.207.
Rodriguez-Gattorno, G., Galano, A., Torres-García, E., 2009. Surface acid-basic properties of WOx-ZrO_2 and catalytic efficiency in oxidative desulfurization. Appl. Catal. B Environ. 92 (1–2), 1–8. https://doi.org/10.1016/j.apcatb.2009.07.031.
Saha, B., Vedachalam, S., Dalai, A.K., 2021. Review on recent advances in adsorptive desulfurization. Fuel Process. Technol. 214, 106685. https://doi.org/10.1016/j.fuproc.2020.106685.
Salah, H.B., Nancarrow, P., Al-Othman, A., 2021. Ionic liquid-assisted refinery processes—A review and industrial perspective. Fuel 302, 121195. https://doi.org/10.1016/j.fuel.2021.121195.
Santos, I.C.M.S., Paz, F.A.A., Simões, M.M.Q., Neves, M.G.P.M.S., Cavaleiro, J.A.S., Klinowski, J., et al., 2008. Catalytic homogeneous oxyfunctionalization with hydrogen peroxide in the presence of a peroxotungstate. Appl. Catal. Gen. 351 (2), 166–173. https://doi.org/10.1016/j.apcata.2008.09.013.
Shafiq, I., Shafique, S., Akhter, P., Ishaq, M., Yang, W., Hussain, M., 2021. Recent breakthroughs in deep aerobic oxidative desulfurization of petroleum refinery products. J. Clean. Prod. 294, 125731. https://doi.org/10.1016/j.jclepro.2020.125731.
Shan, Q., Zhang, J., Wang, Y., Liu, W., 2022. Preparation of ionic liquid-type UiO-66 and its adsorption desulfurization performance. Fuel 312, 122945. https://doi.org/10.1016/j.fuel.2021.122945.
Shiraishi, Y., Tachibana, K., Hirai, T., Komasawa, I., 2002. Desulfurization and denitrogenation process for light oils based on chemical oxidation followed by liquid-liquid extraction. Ind. Eng. Chem. Res. 41 (17), 4362–4375. https://doi.org/10.1021/ie010618x.
Shirley, D.A., Giauque, W.F., 1959. The entropy of Iodine. Heat capacity from 13 to 327 K. Heat of Sublimation. J. Am. Chem. Soc. 81 (18), 4778–4779. https://doi.org/10.1021/ja01527a005.
Tanimu, A., Tanimu, G., Ganiyu, S.A., Gambo, Y., Alasiri, H., Alhooshani, K., 2022. Metal-free catalytic oxidative desulfurization of fuels - a review. Energy Fuel. 36 (7), 3394–3419. https://doi.org/10.1021/acs.energyfuels.1c04411.
Wang, C., Chen, Z., Zhu, W., Wu, P., Jiang, W., Zhang, M., et al., 2017. One-pot extraction and oxidative desulfurization of fuels with molecular oxygen in low-cost metal-based ionic liquids. Energy Fuel. 31 (2), 1376–1382. https://doi.org/10.1021/acs.energyfuels.6b02624.
Wang, Q., Zhang, T., Zhang, S., Fan, Y., Chen, B., 2020a. Extractive desulfurization of fuels using trialkylamine-based protic ionic liquids. Sep. Purif. Technol. 231, 115923. https://doi.org/10.1016/j.seppur.2019.115923.
Wang, Y., Li, H., Zhu, W., Jiang, X., He, L., Lu, J., et al., 2010. The extractive desulfurization of fuels using ionic liquids based on $FeCl_3$. Pet. Sci. Technol. 28 (12), 1203–1210. https://doi.org/10.1080/10916460903066148.
Wang, Y., Liu, W., Zhang, J., Shan, Q., 2022. Preparation of co-schiff base complex and its adsorption desulfurization. Fuel 324, 124696. https://doi.org/10.1016/j.fuel.2022.124696.
Wang, Y., Wu, J., Zhou, E., Wang, J., Li, K., 2020b. Deep oxidative desulfurization of model fuels with sulfonated polystyrene as catalyst in ionic liquids. J. Taiwan Inst. Chem. Eng. 115, 128–134. https://doi.org/10.1016/j.jtice.2020.10.001.
Wang, Z., Ma, W., Chen, C., Ji, H., Zhao, J., 2011. Probing paramagnetic species in titania-based heterogeneous photocatalysis by electron spin resonance (ESR) spectroscopy-A mini review. Chem. Eng. J. 170 (2–3), 353–362. https://doi.org/10.1016/j.cej.2010.12.002.
Wu, J., Wu, X., Zhao, P., Wang, Z., Zhang, L., Xu, D., et al., 2021. Extraction desulphurization of fuels using ZIF-8-based porous liquid. Fuel 300, 121013. https://doi.org/10.1016/j.fuel.2021.121013.
Xing, Y., Yao, Z., Li, W., Wu, W., Lu, X., Tian, J., et al., 2021. Fe/Fe_3C boosts H_2O_2 utilization for methane conversion overwhelming O_2 generation. Angew. Chemie - Int. Ed. 60 (16), 8889–8895. https://doi.org/10.1002/anie.202016888.
Xu, J., Zheng, X., Feng, Z., Lu, Z., Zhang, Z., Huang, W., et al., 2021a. Organic wastewater treatment by a single-atom catalyst and electrolytically produced H_2O_2. Nat. Sustain. 4 (3), 233–241. https://doi.org/10.1038/s41893-020-00635-w.
Xu, L., Luo, Y., Liu, H., Yin, J., Li, H., Jiang, W., et al., 2021b. Extractive desulfurization of diesel fuel by amide-based type IV deep eutectic solvents. J. Mol. Liq. 338, 116620. https://doi.org/10.1016/j.molliq.2021.116620.
Yang, H., Jiang, B., Sun, Y., Hao, L., Huang, Z., Zhang, L., 2016. Synthesis and oxidative desulfurization of novel lactam-based Brønsted-Lewis acidic ionic liquids. Chem. Eng. J. 306, 131–138. https://doi.org/10.1016/j.cej.2016.07.044.
Yin, Y., Xu, Y., Guo, K., Zhang, P., Zeng, Y., 2022. Adsorptive desulfurization using Cu^+ modified UiO-66(Zr) via ethanol vapor reduction. J. Environ. Chem. Eng. 10, 108578. https://doi.org/10.1016/j.jece.2022.108578.
Zhang, R., Goldstein, S., Samuni, A., 1999. Kinetics of superoxide-induced exchange among nitroxide antioxidants and their oxidized and reduced forms. Free Radic. Biol. Med. 26 (9–10), 1245–1252. https://doi.org/10.1016/S0891-5849(98)00328-1.
Zhao, D., Liu, R., Wang, J., Liu, B., 2008a. Photochemical oxidation-ionic liquid extraction coupling technique in deep desulphurization of light oil. Energy Fuel. 22 (2), 1100–1103. https://doi.org/10.1021/ef700668h.
Zhao, D., Sun, Z., Li, F., Liu, R., Shan, H., 2008b. Oxidative desulfurization of thiophene catalyzed by $(C_4H_9)_4NBr \cdot 2C_6H_{11}NO$ coordinated ionic liquid. Energy Fuel. 22 (5), 3065–3069. https://doi.org/10.1021/ef800162w.
Zhao, D., Sun, Z., Li, F., Shan, H., 2009. Optimization of oxidative desulfurization of dibenzothiophene using a coordinated ionic liquid as catalytic solvent. Pet. Sci. Technol. 27 (17), 1907–1918. https://doi.org/10.1080/10916460802653954.
Zhao, D., Wang, J., Zhou, E., 2007. Oxidative desulfurization of diesel fuel using a Brønsted acid room temperature ionic liquid in the presence of H_2O_2. Green Chem. 9 (11), 1219–1222. https://doi.org/10.1039/b706574d.
Zhao, D., Wang, Y., Duan, E., Zhang, J., 2010. Oxidation desulfurization of fuel using pyridinium-based ionic liquids as phase-transfer catalysts. Fuel Process. Technol. 91 (12), 1803–1806. https://doi.org/10.1016/j.fuproc.2010.08.001.
Zhao, R., Wang, J., Zhang, D., Sun, Y., Han, B., Tang, N., et al., 2017. Biomimetic oxidative desulfurization of fuel oil in ionic liquids catalyzed by Fe (III) porphyrins. Appl. Catal. Gen. 532, 26–31. https://doi.org/10.1016/j.apcata.2016.12.008.
Zhou, S., Wu, Z., Liu, J., Wang, Y., Shao, S., Liu, F., et al., 2024. Modifying the active phase structure of Ni_2P/Al_2O_3 by Ga introduction for improved hydrodesulfurization of diesel. Chem. Eng. J. 479, 147776. https://doi.org/10.1016/j.cej.2023.147776.
Zhu, M., Lu, J., Hu, Y., Liu, Y., Hu, S., Zhu, C., 2020. Photochemical reactions between 1,4-benzoquinone and $O_2\bullet^-$. Environ. Sci. Pollut. Res. 27 (25), 31289–31299. https://doi.org/10.1007/s11356-020-09422-8.
Zhu, X., Bi, Q., Yang, L., Xing, H., Wang, L., Rong, M., et al., 2021. Control of metal-support interaction in magnetic MoS_2 catalyst to enhance hydrodesulfurization performance. J. Environ. Chem. Eng. 9 (5), 106109. https://doi.org/10.1016/j.jece.2021.106109.